Hydromechanical assessment of a complex landslide through geophysics and numerical modeling: Toward an upgrade for the Villerville landslide (Normandy, France)

Guillaume Thirard, Yannick Thiery, Sébastien Gourdier, Gilles Grandjean, Olivier Maquaire, Benjamin François, Adnand Bitri, Salimata Coulibaly, Candide Lissak, Stéphane Costa

Hydromechanical assessment of a complex landslide through geophysics and numerical modeling: toward an upgrade for the Villerville landslide (Normandy, France)

Guillaume Thirard[*1,2], Yannick Thiery[2], Sébastien Gourdier[2], Gilles Grandjean[2], Olivier Maquaire[1], Benjamin François[2], Adnand Bitri[2], Salimata Coulibaly[2], Candide Lissak[1], Stéphane Costa[1]*

[1]NORMANDIE UNIV, UNICAEN, CNRS, LETG, 14000 CAEN, France

[2]Bureau de Recherches Géologiques et Minières (BRGM), 3 avenue Claude Guillemin - BP 36009 - 45060 Orléans Cedex 2, France

***Contact:** guillaume.thirard@unicaen.fr

Abstract

The Pays d'Auge (Normandy, France) is impacted by large deep-seated landslides along its coastline. The largest of these landslides, the "Cirque des Graves", has been studied since the 1980s because of significant stakes in the active zone. To characterize the hydromechanical functioning of the central part of the cirque, which is the most active part and includes the majority of the issues at stake, we performed new investigations that complement prior studies. Through the joint use of high-resolution geophysics (seismic refraction and ERT) coupled with geotechnical knowledge, a geometric model was highlighted on a large profile. Then, the mechanical behavior and slope stability were assessed by finite-difference numerical modeling (FDM) with FLAC2D®. To calibrate the model, a back-analysis was first realized on an eastern profile, for which the geometry and slip surfaces were identified by field surveys. The agreement of the model results on the eastern profile constrained by inclinometry enables a transposition of the geomechanical parameters on the central profile to assess its functioning and to locate the areas subject to mechanical weaknesses. A translational movement was revealed at the upstream end of the landslide, as well as nested roto-translational envelopes in the downstream two-thirds of the landslide. These results allowed robust assumptions with regard to the location of the slip surfaces and the zones undergoing stress-strain. The influence of groundwater was also assessed and discussed with respect to the overall slope stability. This study demonstrates the pros and cons of conventional finite difference modeling, as well as of

back-analysis by parametric transposition. The benefits of the joint use of geophysical methods and numerical modeling were also highlighted and discussed.

Keywords: landslide, geophysics, numerical modeling, Mohr-Coulomb, hydromechanics

1. Introduction

Deep landslides usually occur in complex lithological structures, with long-term kinematic and multiple triggering factors (Hungr et al., 2014; Malamud et al., 2004; Shi et al., 2020). Understanding their internal structure and hydromechanical behavior is essential to understand their dynamics (velocity, rate of evolution, subsurface flows, etc.) and to better manage hazards.

For this purpose, geophysical methods are powerful in revealing the stratigraphic complexity and saturation of formations (Caris and Van Asch, 1991). Among classical geophysical methods, electrical resistivity tomography (ERT) and seismic refraction are among the most widespread for the study of gravitational hazards (Grandjean et al., 2006; Jongmans and Garambois, 2007; Meric et al., 2005; Whiteley et al., 2019). They are frequently used together due to the limitations of each approach (Chen et al., 2019; Coulouma et al., 2012; Pazzi et al., 2019).

These methods are easy to implement but require in situ data and sufficiently good knowledge of the geological context to interpret the results (Gilli et al., 2008). In particular, empirical data (borehole logs, piezometry, inclinometry, etc.) provide reliable information on the structure and hydrology of the slope (Perrone et al., 2014). Relationships can then be found between geophysical data and geotechnical slope parameters (resistivity and seismic velocity) to help with interpretation (Denchik et al., 2019).

When the knowledge is sufficiently good to propose a complete functioning model of a landslide, stability assessment can be undertaken by calculating the limit equilibrium of the slope. In geoengineering, stability is commonly expressed by a factor of safety (FoS) calculation for different potential failure mechanisms (Duncan, 1996; Malet et al., 2005). This coefficient is defined as the ratio of the shear strength of the terrain to the stress it undergoes (Maquaire, 1990; Michalowski, 2002; Zhang et al., 2013). Stability calculations and stress-strain state can be performed using two- or three-dimensional numerical models (Berthaud et al., 2018; Plumelle et al., 2013).

Among others, limit equilibrium (LEM), finite element (FEM), finite difference (FDM) and discrete element (DEM) methods are widely used for the understanding and management of landslides (Brideau et al., 2006; Chen and Yuan, 2012; Dawson et al., 1999; Duncan, 1996; Li and Wang, 2020; Liu et al., 2020; Lu et al., 2014; Shen et al., 2012; Tang et al., 2009; van Asch et al., 2007). These models are classical models in operational engineering and in the framework of geotechnical, civil engineering or even mining engineering expertise. An elasto-plastic approach is generally used, considering a plastic limit condition (Mohr-Coulomb criterion) and a plastic strain localization condition (Lignon et al., 2009; Rice, 1976). Mohr-Coulomb criterion allows us to assess shear failure mechanisms considering the parameters of the internal friction angle ϕ' and associated effective cohesion C' (Arthur et al., 1977). In addition, it is considered suitable for studying the porous and plastic behavior of clays (Krabbenhøft et al., 2008).

However, deep landslides with complicated structures sometimes remain difficult to grasp using classical modeling methods due to their complex kinematics and hydrological features (Cambou et al., 2019; Lignon et al., 2009; Mergili et al., 2014). This type of landslide is frequently studied internationally (Deiana et al., 2020; Van Den Eeckhaut et al., 2009; Zêzere et al., 2005; Zhang et al., 2017), which raises the question of the relevance of using such models in engineering for this type of gravitational phenomenon. This is a central issue because the characterization of their hydromechanical behavior is crucial for better management of areas prone to hazards (Lollino et al., 2014).

Based on these considerations, this article focuses on the identification of the hydromechanical behavior of a large landslide, the Cirque des Graves (Normandy, France). A multimethod approach based on geophysics and geotechnical modeling is implemented on this landslide, which has been instrumented for several decades. Finite difference modeling (FDM) is used to understand the main physical processes, and its pros and cons are discussed. The modeling software FLAC© is chosen because of its capability to assess stress-strain fields and to determine the slip surface without *prior* knowledge.

By using interdisciplinary and complementary methods, this work aims to provide answers to the following questions: How far can we go in the assessment of a complex slope with the classical FDM method? Can shear surfaces be reproduced in a complex environment? Can the sensitivity of the slope to water be reliably determined? Finally, can good empirical knowledge compensate for the possible shortcomings of the model in the determination of hydromechanical behavior?

A back-analysis was first performed on a well-constrained profile located east of the landslide (calibration profile, figure 1B), for which the slip surface was numerically reproduced. Once the geomechanical parameters are calibrated, transposition is carried out on the median part of the landslide. This area is known to be hydrologically and kinematically very sensitive (Thirard et al., 2020). In contrast, the transposition profile is not structurally constrained. To gain better insight into its structure and geometry, new geophysical acquisitions were carried out. The results of geophysical interpretations complete the available field data and are compared with the results of the numerical models, allowing strong assumptions regarding the hydromechanical functioning of this specific part of the landslide.

2. Description of the study site

The Cirque des Graves is a coastal landslide located along the English Channel at the northern limit of Pays d'Auge in Normandy (Figure 1). The Pays d'Auge is at the junction of an ancient crystalline massif to the west (Armorican Massif) and a more recent sedimentary basin to the east (Parisian Basin) (Elhaï, 1963). This location induced carbonate and terrigenous sedimentary alternations, which explain the complex stratigraphy. The regional dip is 1°E.

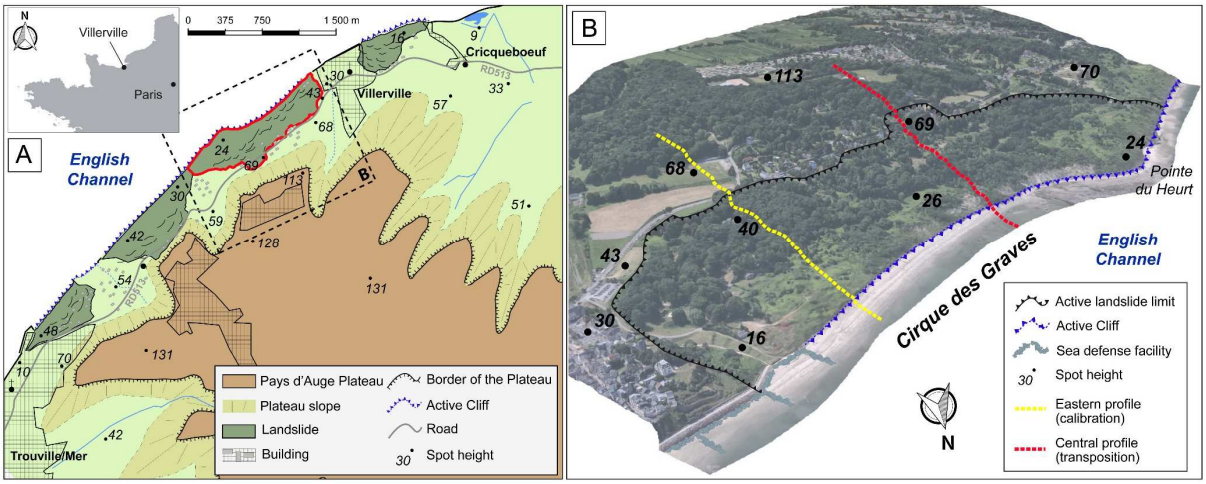

Figure 1- Location of the study site. (A) Location of the unstable zones on the northern edge of the Plateau d'Auge and the Cirque des Graves, (B) area of the Cirque des Graves landslide and location of the geophysical investigation transect in the median part of the unstable zone.

The Jurassic formations are characterized by marl and limestone deposits (Dugué, 1991; Elhaï, 1963). At the bottom, the Hennequeville limestone (early Oxfordian) is the lower limit of the landslide (Flageollet and Helluin,

1987; Maquaire, 1990). The Hennequeville Formation is overlain by marl and clay formations from the late Oxfordian and Kimmeridgian.

Above, the Cretaceous formations are discordant and mainly composed of ferruginous and glauconitic Albian sands. Then, Cenomanian chalk is found, with a heterogeneous state of weathering (Figure 2).

At the edge of the plateau, the chalk splits into slabs of varying size through dissolution and fracturing. Between these slabs are located surficial formations or "heads" (Maquaire, 1990). They consist of a mixture of colluvium, loess and chalk decalcification products (i.e., clay-with-flints) (Lissak, 2012; Maquaire, 1990).

The alternation between loose and coherent layers with various degrees of weathering has favored the triggering of landslides. At the edge of the Plateau d'Auge, there are four large landslides that were initiated at the end of the Weichselian period (Elhaï, 1963; Journaux, 1971). The Cirque des Graves is the most extensive of these landslides, with an area of 47 ha. Because of permanent marine erosion at the foot of the slope, stability cannot be reached (Flageollet, 1992).

This landslide is deep with multiple slip surfaces and is subject to retrogressive dynamics (Journaux, 1971; Lissak, 2012; Maquaire, 1990). In the last 30 years, scientific research has proven hydrological control and a direct link between water table levels and extreme or seasonal movements (Bogaard et al., 2013; Lissak et al., 2014a; Maquaire, 1990). Topographic readjustments have occurred as a result of piezometric variations in the chalk aquifer, with more sudden accelerations, such as in 1982, 1988, 1995 and 2001 (Lissak, 2012). Previous studies have shown that these violent movements were related to the development of deep slip surfaces in the Kimmeridgian and Oxfordian layers (Maquaire, 1990).

The functioning of the eastern part of the Cirque was also better constrained, as it had major infrastructure until the 1990s (Flageollet and Helluin, 1987; Lissak, 2012; Maquaire, 2000, 1990; Pareyn et al., 1982). The former developments in this eastern part, consisting mainly of individual dwellings and a campsite, were gradually removed due to land instability. Currently, this area is a park for recreational use only, and no infrastructure is currently inhabited. Geotechnical and geophysical surveys have also been conducted on other areas of the landslide, but they were more widespread (Lissak et al., 2014b).

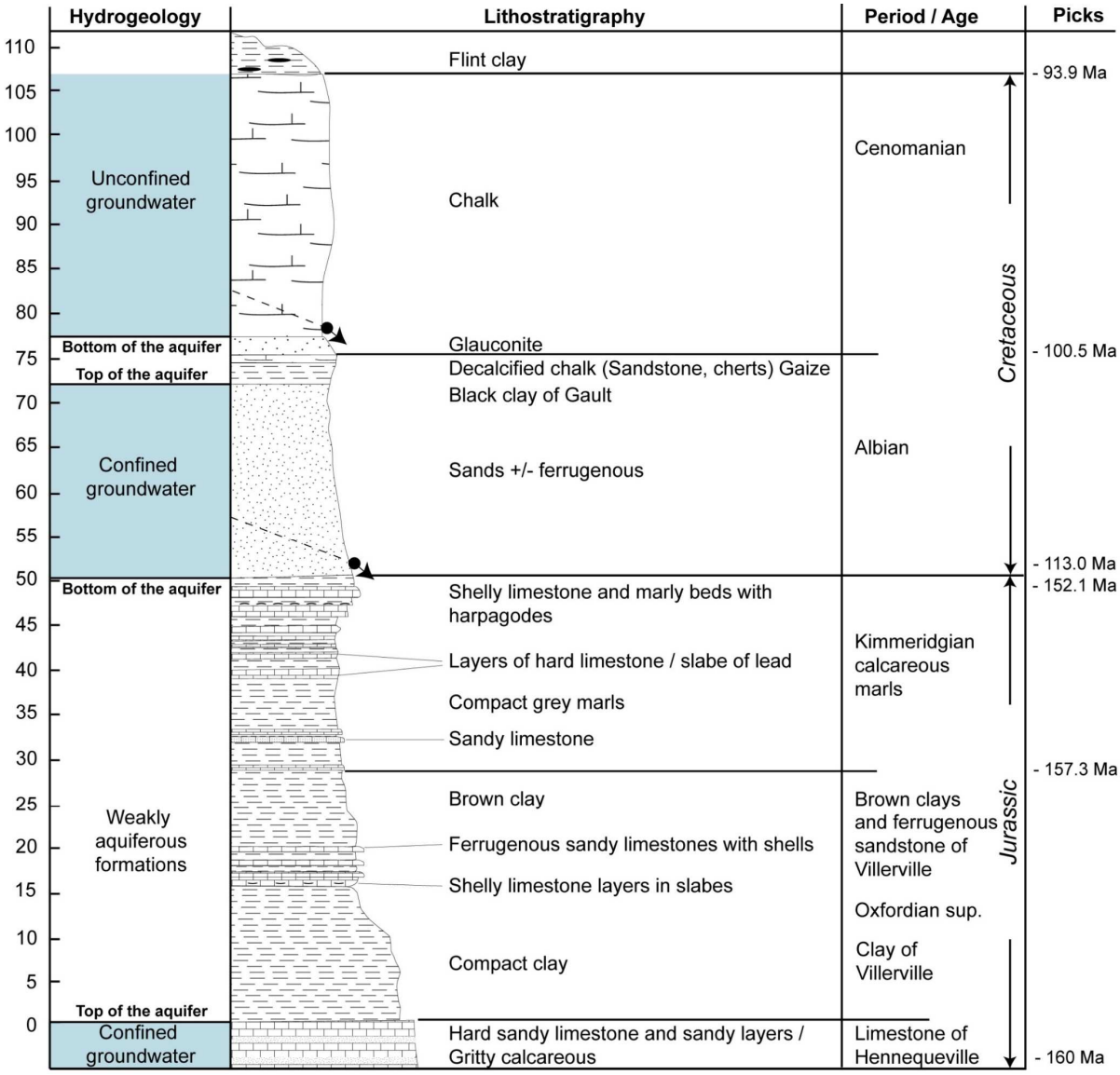

Figure 2- Lithostratigraphic section and associated aquifer potential on the plateau in the vicinity of Villerville (modified from Sinelle, 1989). Deep-seated landslide surfaces are typically developed in formations with low aquifer potential in Jurassic deposits (Kimmeridgian/Oxfordian).

More recent research showed that the central part of the landslide, which now concentrates the most economic and human issues, is also the most active zone from a kinematic and hydrodynamic perspective (Thirard et al., 2020). This research has revealed a major interest on this central part for several reasons : 1- this area is the furthest back from the unstable zone; 2- this area is the most active of the landslide; 3- it is subject to a preferential discharge of the continental water table upstream; 4- there is resurgences at the mid-slope and at the bottom of the slope; 5- this area is affected by marl flows downstream (Figure 3c); and 6- this area has strategic, economic and human issues (housing, tourist road, and networks).

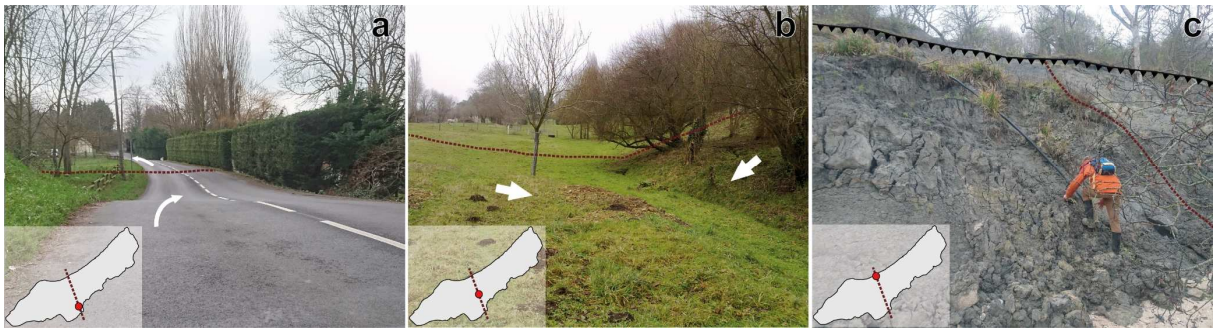

Figure 3- Morphology of the investigated profile. The brown dashed line symbolizes the profile alignment. (a) Multiple collapses of RD513 upstream of the landslide; (b) slope/counterslope morphology (arrows) below a dwelling with the presence of a drainage network in the thalweg; and (c) marl-clay chaotic bedding at the foot of the slope.

In this part of the Cirque, the impact of landslide activity is noticeable on facilities, particularly on the tourist road located upstream of the active part of the slide (RD513), which requires frequent restoration (Figure 3a). Several residential buildings are also located there, some of which show damages (cracks, tilting of the building, etc.), which induces human issues beyond the material aspect.

3. Material, methods and model calibration

After presenting the main features of the landslide and associated issues, this section aims to present the multi-disciplinary methodology implemented.

Several preliminary steps are necessary before being able to evaluate hydromechanical functioning (Figure 4). First, a geotechnical synthesis allows the establishment of realistic values for each formation. These values then enable parameterization of the back-analysis profile (eastern cross-section), for which the geometry of the formations and slip surfaces are known. Once these two preliminary steps are completed, the geomechanical values retained are transposed to the central cross-section investigated.

ERT and seismic refraction surveys are then carried out on this second profile. After inversion and interpretation, this aims to provide information for establishing a new geometric model. Finally, this new model and the geomechanical parameters retained on the eastern profile enable the achievement of the numerical model by FDM on the transposition profile in the central part. The methodological choices and the techniques used are described below.

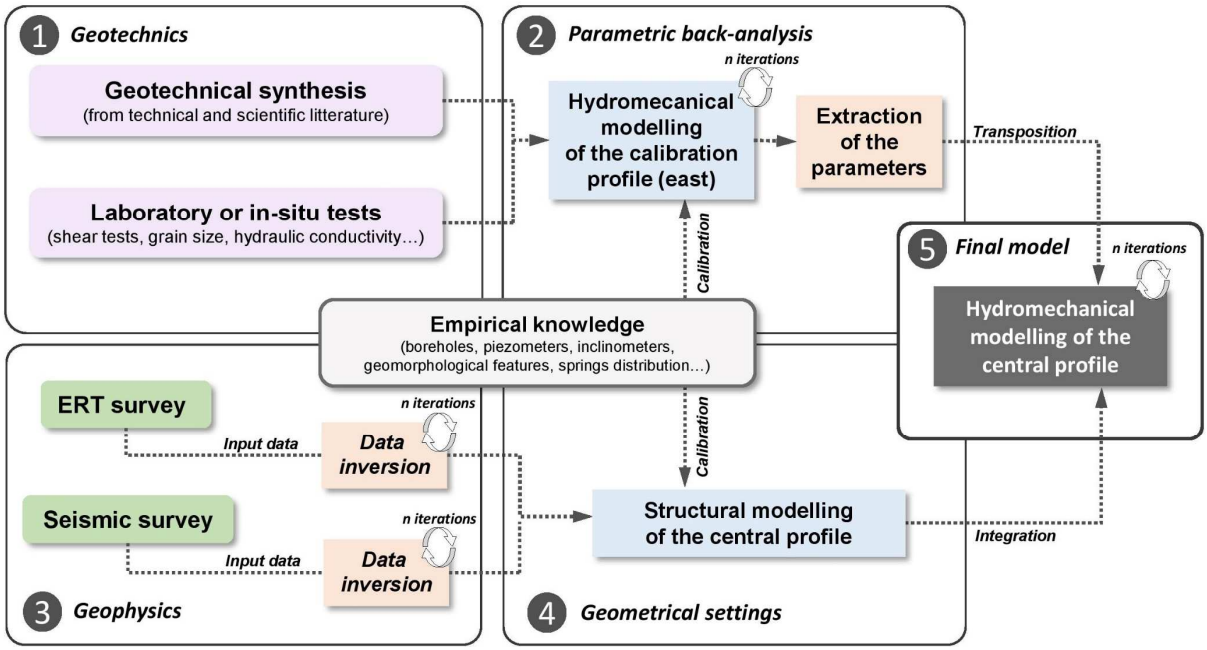

163

164 *Figure 4- Methodology of the study.*

165

166 **3.1 Summary of geotechnical parameters**

167 The definition of the possible ranges of the different geomechanical parameters is the first step for the setting of
168 numerical models. A series of geotechnical studies are carried out in the context of development work, opera-
169 tional geotechnical studies and scientific research.

170 The geomechanical and hydraulic values from laboratory tests identified in geotechnical reports are summarized
171 in table 1, which aims to highlight the ranges of characteristic values for each geological layer.

172

173 *Table 1- Summary of the main characteristics of the materials found in the Cirque des Graves.*

Parameter	*Sym-bol*	*Unity*	*Surficial formation (1)*		*Chalk +/- weathered (2)*		*Glauconitic Sand (3)*		*Undisturbed Clay-marl (4)*		*Disturbed Clay-marl (5)*	
No. of samples	-	-	25		41		13		28		17	
-	-	-	Min	Max	Min	Max	Min	Max	Min	Max	Min	Max
Sat. hydraulic conductivity	Ksat	m/s-1	1.5E-8	2.0E-7	2.0E-7	1.2E-4	1.5E-7	1.8E-4	5.7E-9	7.5E-8	1.4E-7	2.7E-6
Natural Water content	ρ	%	23.6	52.0	16.5	37.3	21.3	38.9	18	30	18	40
Angle of friction	ϕ'	(°)	15	25	19	36	29.5	35	15	26	7	19
Cohesion	C'	kPa	0	7	10	60	0	6.5	10	122	0	30
Saturated volu-metric weight	ρsat	kg/m^3	1530	1980	1500	2400	1271	2000	1800	2040	1800	1880
Dry volumetric weight	ρd	kg/m^3	1210	1590	940	1750	955	1650	1485	1672	1380	1500
Liquid limit	LL	%	41	68	73*		-	-	50	92	89*	
Plastic limit	LP	%	23	46.5	43*		-	-	31	55	38*	
Plasticity index	IP	-	15	27	30*		-	-	17	37	51*	

Methylene blue	Vb	-	-	-	4.4*	-	-	1	7.8	-

* Unique laboratory test

(1) (Bergin, 1972a, 1972b; Hydrogeotechnique, 2006a; IMSRN, 2005; Prunet, 2001)

(2) (Bergin, 1972a, 1972b; Evrard and Sinelle, 1980; Hydrogeotechnique, 2007, 2006a, 2006b; Lissak, 2012; Unisol, 2009)

(3) (Bergin, 1972b; Fressard, 2013; Lissak, 2012; Unisol, 2009)

(4) (Fressard, 2013; Hydrogeotechnique, 2006b, 2006a; IMSRN, 2005; Maquaire, 1990)

(5) (Bergin, 1972a; CETE, 1978; Lissak, 2012; Maquaire, 1990)

The number of tests carried out is uneven but remains sufficient to define representative ranges of values. A total of 124 laboratory tests are identified (all methods combined), including 45 for marl-clay materials. The Hennequeville limestone cannot be characterized, which is not an issue because this layer is very cohesive and not affected by the landslide (Maquaire, 1990).

The results of the shear tests carried out show classical plastic behavior for most formations, particularly for clays and marls. Most materials in the Cirque des Graves have a friction angle range from 20 to 25° for peak values under drained conditions. Only the Albian sands show more frictional behavior (29.5–35°) and nearly nil cohesion (0–6.5 kPa). In general, the cohesion shows low values (< 10 kPa), except for the chalk (10–60 kPa) and sound marl-clay (10–122 kPa).

The properties of clay marls are progressively reduced by reactivations along the slip surface (Maquaire, 1990). This behavior is crucial because it favors reactivations along existing envelopes. Alternating and long-term shear tests clearly show a decrease in the residual effective cohesion and friction angle (C'_{res}/ ϕ'_{res}) after prolonged loading (Figure 5). The median cohesion decreases sharply from 66 to 6 kPa. At the same time, the mean friction angle is lowered by approximately 10° from 20.4 to 11.6°. This behavior is common for this type of material (Alonso and Pinyol, 2015; Hutchinson et al., 1973; Maquaire, 1990), but this downgrade in mechanical properties should be considered in the model settings.

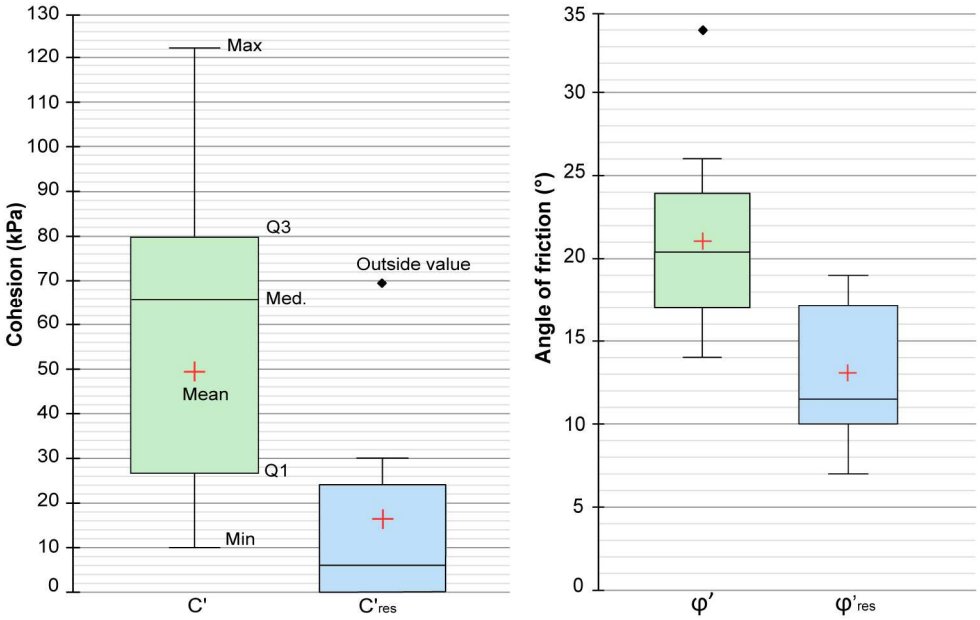

Figure 5 - Evolution of the cohesion and friction angle of clayey marly formations for direct simple shear tests (green box-plot) and for long-term alternating tests for residual values (blue boxplot).

The parameters resulting from this synthesis are relevant to the determination of the material's plasticity criteria, in particular those involved in Mohr-Coulomb theory. Beyond the plastic behavior, the elasticity is generally considered by FDM through the joint use of bulk and shear modulus. An alternative input is also possible by using the elastic modulus (or Young modulus) and Poisson ratio. In our case, the elastic properties are not characterized by laboratory tests. The values are therefore approximated using those proposed for similar materials in the software database. This allows us to approximate the behavior of the materials while using realistic plastic characteristics for each lithology. The chosen values are presented in table 4.

3.2. Back-analysis on the eastern profile

3.2.1. Prior knowledge and lithological modeling

Once the parameter ranges are assessed, then it is possible to numerically attempt to reproduce the eastern profile to calibrate the model parameters for the central profile.

The slip surfaces were already characterized in the eastern part of the cirque along a profile using three inclinometers (Maquaire, 1990). These devices reach down to the Hennequeville limestone bedrock and are located upstream, center and downstream of the slope (Figure 6). This enables us to constrain the deep surface of the

landslide along the entire length of the slope at depths varying from -23 m upstream to -14.5 m downstream (Figure 6). The shape of the envelope, although constrained at these three inclinometers, is not known with certainty. It may have a more or less curvilinear or flat tendency depending on the hypotheses considered or even a complex geometry with successive interlocking (Flageollet and Helluin, 1987; Maquaire, 1990).

The boreholes drilled to install the inclinometers allow us to determine the lithology of the profile. A geometric model was initially proposed by Maquaire (1990) based on these implementations. This initial geometry was then refined by means of electrical tomography surveys and by additional boreholes installed between 1990 and 2012 (Lissak, 2012).

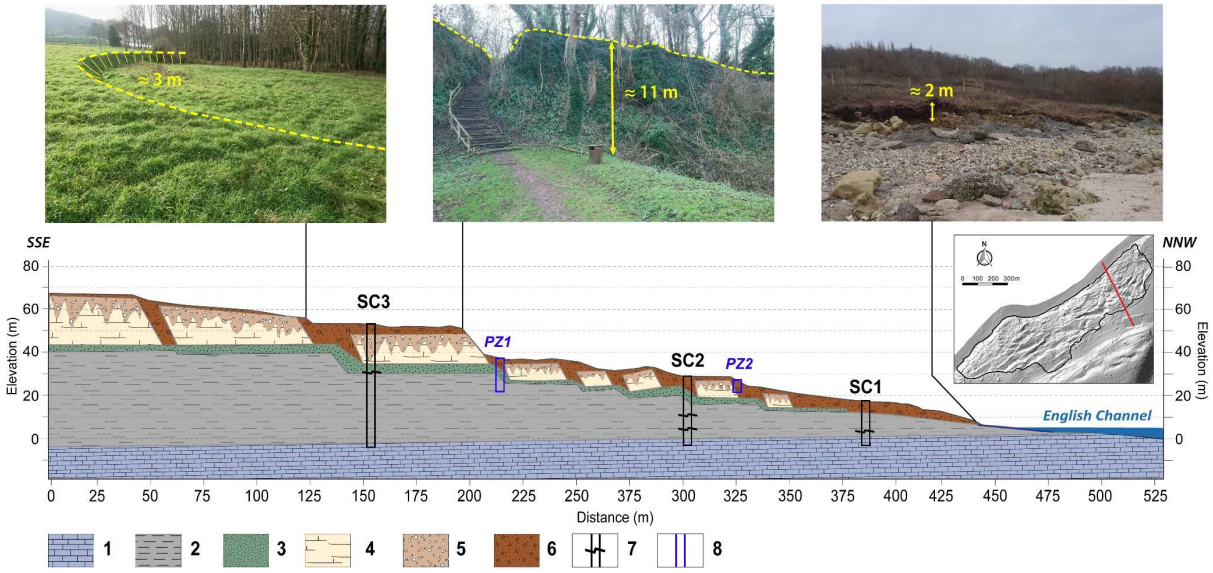

Figure 6- Geometric model interpreted from the work of Maquaire (1990) and Lissak (2012) for the Parc des Graves profile. Legend: (1) limestone; (2) marl/clay; (3) glauconitic sand; (4) chalk; (5) weathered/decalcified chalk; (6) surficial and infill formations; (7) inclinometer and characterized rupture; and (8) piezometer.

Thanks to the geometric model and a constrained deep slip surface at several points, a back-analysis can be performed on the geomechanical parameters. This method is proven and frequently used for the calibration of numerical models (Deschamps and Yankey, 2006; Zhang et al., 2013). It needs some empirical knowledge to be reliable (Hürlimann, 2000; Malet, 2003; Tang et al., 1999), which is the case here.

3.2.2. Numerical modeling with FLAC®

Modeling is realized with FLAC® (Fast Lagrangian Analysis of Continua) (Cundall et al., 1993; Itasca, 2019) version 8.1, which uses the explicit finite difference method and enables the derivation of equations in the com-

pletion of variables (Itasca, 2019) and allows the stress-strain fields and the associated displacements to be calculated for each node of the mesh. It has the advantage of estimating the areas subjected to compression, tension or shear at each iteration and at each node of the model. This software is proven for the assessment of landslide phenomena (Chen and Yuan, 2012; Dawson et al., 1999; Floris and Bozzano, 2008; Shen et al., 2012; Xu et al., 2014; Zhou et al., 2013). FLAC® uses the strength reduction method (SRM) based on the iterative reduction of cohesion and friction angle until the state of limit equilibrium is obtained (Dawson et al., 1999; Itasca, 2019).

A five-layer model is realized to numerically reproduce the slip surface characterized by inclinometry. This model incorporates a discretization of the different chalk slabs (Figure 7) and allows us to characterize the zones prone to stress that may affect the formations surrounding the blocks, in particular the surficial formations and sands, which are responsible for readjustments and tilting of chalk slabs. It also allows the identification of possible secondary mechanical weaknesses.

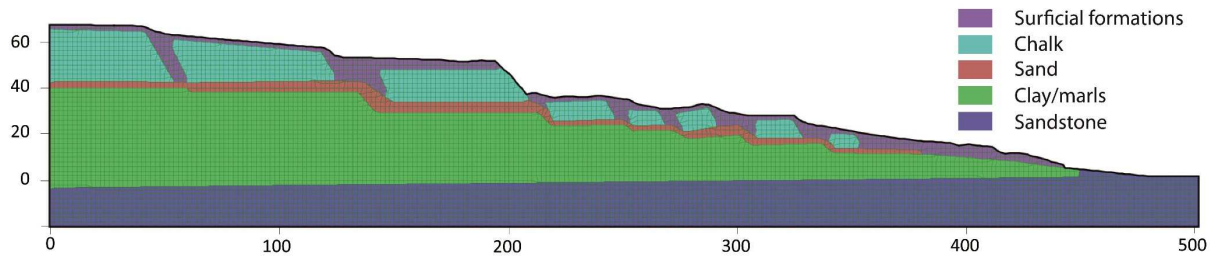

Figure 7- Geometry of the mesh in five classes for the eastern profile of the Cirque des Graves (calibration profile) produced with FLAC®.

The two-dimensional primary elements of FLAC® are quadrilaterals with four nodes. The size of the mesh formed by these nodes is strategic because it attempts to find the optimum between the calculation time and targeted result (Touitou, 2002). After several tests, a regular cell size of 1 m is applied to the entire model, which allows us to consider the thinness of some layers (sands and surficial formations) while maintaining a reasonable calculation time for each run.

Since the mode of failure by shearing is attested in the landslide, Mohr-Coulomb criterion is suitable. The values retained for clays and marls are those of residual tests (ϕ'_{res} / C'_{res}) to take into account the erosion of the materials by successive reactivation of the slip surface (Flageollet and Helluin, 1984; Maquaire, 1990; Maquaire and Gigot, 1988). As the landslide is continuously active throughout the year, the residual values are considered relevant.

Due to the heterogeneity of the chalk in regard to the weathering and the fissural network, the geomechanical characteristics are reinforced to consider a homogeneous and cohesive material. The density is, however, in accordance with laboratory tests to apply a realistic normal stress. Although no laboratory tests were conducted on the limestone, it is set as cohesive and frictional to be considered stable bedrock.

Boundary conditions are applied at the limits of the model (sides and bottom) to allow the calculation of stress in the entirety of the mesh. No numerical interfaces are applied. The aim is to let the model calculate the plasticity and shear stress, without any operator influence. To ensure that the boundary conditions do not influence the numerical calculations in the active area, the model is extended upstream and downstream.

3.2.3. Piezometric parameterization

The piezometric level integrated in FLAC® was previously defined using SEEP/W® extension of the Geostudio® software (Krahn, 2004). Various piezometric levels were defined considering a succession of steady states under different water pressure conditions.

The chosen piezometric scenario is selected thanks to reference levels measured during two major crises during which the limit equilibrium was raised. Piezometer PZ1 (Figure 6) reached an extreme reference level of -0.39 m in January 2018. At the same time, cracks appeared along RD513, located upstream of the landslide. Piezometer PZ2 (Figure 6) was monitored during a major acceleration in February 1988 (Lissak, 2012), when the water table increased to a level of -2.87 m. The piezometric scenario closest to these two measurements is selected as a reference for the back-analysis.

3.3. Geophysical acquisitions and geometry of the central profile

Once the calibration profile is modeled and the appropriate parameters are determined, transposition to the central profile can be undertaken, which requires the establishment of a geometric model. For this purpose, two geophysical surveys (ERT and seismic refraction) were carried out. These surveys were conducted at the end of the summer under dry conditions (low piezometric levels).

3.3.1. Electrical resistivity tomography

Monitoring was performed using the "Syscal Pro" multielectrode system, and the measurements were duplicated in a dipole-dipole configuration with an interelectrode spacing of 2.5 m and then in a Wenner-Schlumberger configuration with a spacing of 5 m. These configurations are commonly used in the study of landslides (Pasierb et al., 2019; Van Den Eeckhaut et al., 2007). The dipole-dipole provides information on vertical structures at high resolution, but its depth of investigation is limited due to a weaker signal (Travelletti, 2011). The Wenner-Schlumberger device is less sensitive to vertical and horizontal variations in resistivity and allows a greater depth of investigation (Lissak, 2012; Travelletti, 2011).

The measurement was carried out using five electrode streamers progressively offset to cover a total distance of 445 m from upstream to downstream. The location of the electrodes was surveyed with a Trimble Geo7X GPS.

Once the acquisition was completed, the inversions were conducted with RES2DINV (Loke, 1999; Loke and Barker, 1996). To obtain a fine resolution in the near surface while imaging deeper formations, the 2.5 and 5 m acquisitions were merged. Dipole-Dipole data were kept at the surface, and Wenner-Schlumberger data were kept at depth. An inversion based on the $_{L1}$ regularization norm ("robust" and "blocky") was then applied using the least squares method and a data constraint factor of 0.05 (Loke et al., 2003). The robust inversion is suitable due to the sharp lithological changes encountered between chalk, sand and clayey-marl materials, as it better reflects the horizontal boundaries between the formations (Cebulski et al., 2020).

All acquisition and inversion parameters are summarized in table 2.

Table 2- Acquisition and inversion parameters for the high-resolution seismic survey of the Cirque des Graves. WS: Wenner-Schlumberger; and DD: dipole-dipole.

Parameter	***Value***
Profile length (m)	445
Electrode number (WS config)	89
Electrode number (DD config)	168
Electrode spacing (WS config)	5
Electrode spacing (DD config)	2.5
Inverting iterations	4
Data constraint factor	0.05
Minimum damping factor	0.02
Topographic elevation (in m)	[0–78]

The output model enables imaging resistivities over 80 m thick in the middle of the profile. The interpretation was set from three borehole logs carried out on and near the profile.

3.3.2. Seismic refraction

Seismic surveys were used to characterize slip surfaces and image the boundaries between the formations. Seismic surveys are also sensitive to the presence of water and help to differentiate saturated areas, in which the velocity increases strongly. The depth of investigation and sharpness of the recordings relate to the seismic source type (Bitri et al., 1996). The survey was carried out at low tide with a 'double-sledgehammer' type source because of the complexity of access in some parts of the transect (scarps and dense vegetation cover). The geophones have a resonance frequency of 10 Hz and were spaced 2 m apart. Shots were fired every 4 m along the transect. The parameters of the acquisition device are summarized in table 3.

Table 3- Acquisition parameters for the high-resolution seismic survey in the central part of the landslide.

Parameter	***Value***
Profile length (m)	344
Data number	536
Source number	87
Seismic receivers	168
Source spacing (in m)	4
Receiver spacing (in m)	2
Receiver frequency (in Hz)	10
Topographic elevation (in m)	[0–68]
Iterations	13
Damping factor	5
RMS of the final model (in s)	0.05556

The inversions were conducted with MATLAB Tomography Software (Gance, 2014; Gance et al., 2012) using the quasi-Newton algorithm (Gance et al., 2012). This algorithm aims to iteratively minimize the cost function to reduce the residuals between the observed and computed data vectors (Gance, 2014). It uses Fresnel volumes as an approximation to the gradient (Carlier et al., 2018; Gance et al., 2012). It thus enables an increase in the depth resolution without causing divergence during the inversion, allowing us to better resolve the deep layers than a classical algorithm. This recent method has the advantage of being able to image complex structures with several layers with high seismic velocities, which are hidden with classical inversion methods.

Between the initial and final models, thirteen iterations were carried out. The final RMS error of the survey is 0.05 s. The seismic profile is approximately 100 m shorter than the ERT profile upstream. This is due to the presence of a pond upstream of RD513 at the bottom of the rearmost scarp of the slide, which does not allow shooting near the geophones. The final result of the inversion image is the seismic velocity in the landslide over a thickness of approximately 50 m over a major part of the unstable zone, from the foot of the slope to RD513.

3.4. Modeling of the central profile

The creation of the numerical model from geophysical data was set up with FLAC® by applying the geomechanical parameters resulting from the back-analysis carried out on the eastern profile. The same discretization in five lithological classes was applied to this second profile.

The piezometric level was also set with SEEP/W®. The levels were simulated in steady state for several groundwater scenarios because no triggering threshold is known in this part of the landslide. Calculations were carried out for upstream water levels between 90 and 116 m NGF, corresponding to extremely low water levels (emptying of the chalk groundwater and high water levels (almost complete saturation of the slope). Iterative calculations were carried out, successively increasing the upstream level by two meters, to characterize the influence of the groundwater level on the factor of safety of the entire slope.

A delay varying from one to four days was highlighted between rainfall and the response of groundwater fluctuations by Lissak (2014a). It expresses a delay in recharge and then emptying of the aquifers. The deep character of this slide and prior knowledge allow us to approximate its operation by considering a triggering mainly conditioned by the water table levels and upstream inputs.

4. Results

This section presents the results from the geomechanical calibration with FLAC® based on the back-analysis profile located east of the landslide.

Once the calibration is achieved, the results of the geophysical investigations are described on the central profile. Then, the geometric model realized from these geophysical datasets and borehole logs is presented. Finally, the results of the stability assessment with FLAC® are detailed on this central profile.

4.1. Back-analysis and geomechanical parameterization

The limit equilibrium of the slope fits with a piezometric level of a 6 m depth upstream of the model. For this scenario, the differences are 8 cm at PZ1 (-0.39 m measured and -0.31 m modeled) and 4 cm at PZ2 (-2.87 m measured and -2.83 m modeled; Figure 8). This groundwater scenario is therefore defined as a reference for the back-analysis to determine the parameters allowing us to reach FoS = 1.

A series of numerical calculations was undertaken to test the value ranges from the geotechnical synthesis (table 1) until the stability threshold was reached. The geomechanical values retained at the end of this phase are listed in table 4.

Figure 8 shows the results obtained on the eastern profile for the retained parameters. The areas subjected to stresses are expressed by the maximum shear strain rate (Max SSR). The shear strain rate tensor is a relative value derived from the nodal velocities for a sum of averaged subzones. A correspondence is shown between the simulated slip surfaces and the failure zones of the three inclinometers, SC1, SC2 and SC3, without applying any interface on the mesh. The failures are confirmed between -14 and -23 m.

Table 4- Final geotechnical values retained for materials in FLAC® modeling.

Geotechnical parameter	***Symbol***	***Unity***	***Surficial formations***	***Chalk***	***Sands***	***Clay/marls***	***Limestone***
Specific weight	γ	kg/m3	1 700	2 100	1 900	2 000	2 300
Angle of friction	ϕ'	Degrees	17.5	27.8	33	13.5	27.8
Cohesion	*C'*	Pa	7000	6.72e06	3000	5.00e03	6.72e06
Bulk modulus	*K*	Pa	2.67e07	2.26e10	1.33e07	4.00e08	2.26e10
Shear modulus	*G*	Pa	1.60e07	1.10e10	8.00e06	2.40e08	1.10e10
Young's modulus	*E*	Pa	4.00e07	2.80e10	2.00e07	9.5e07	2.80e10
Poisson's ratio	*v*	-	0.30	0.30	0.30	0.30	0.30

At SC3, failure occurs at the contact between the sands and clays. The slip surface then propagates into the clayey marly formation and splits SC2 and SC1 closer to the limestone bedrock. The envelope presents a slight camber downstream of the main scarp (X=200–325 m) and then becomes more linear downstream of SC2 due to the proximity of the limestone. This layer limits its extension at depth.

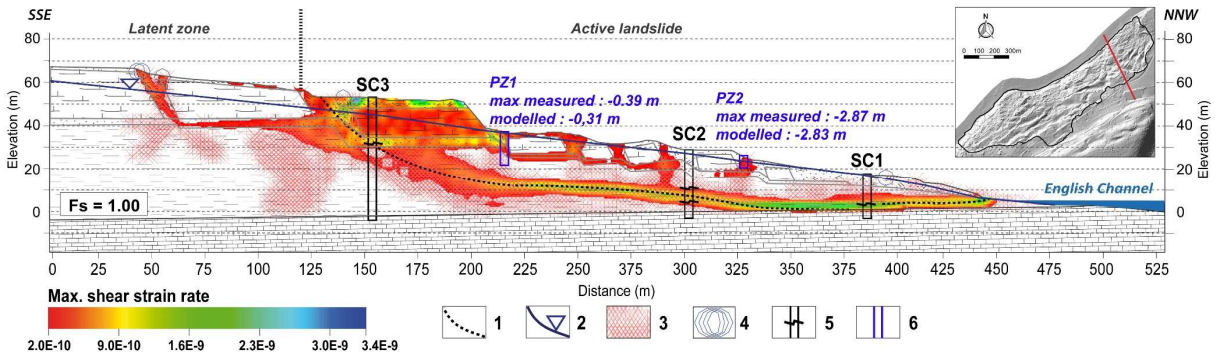

Figure 8- Results of the FLAC® model at equilibrium for the calibration profile, eastern Cirque des Graves. Legend: (1) assumed slip surface; (2) piezometric level simulated with SEEP/W®; (3) shear/compression plasticity criterion exceeded; (4) tensile plasticity criterion exceeded; (5) inclinometer and measured shears; and (6) piezometers.

At the surface, the plastic limit is exceeded in the surficial formations and sands, with increasing shear rates upstream. The main scarp slab, which was set into motion during the event of 2001 (Figure 6), shows a high internal and surrounding shear rate (mainly in sands and surficial formations). Finally, the plasticity threshold is also reached around the slab located upstream of the current active zone (X = 50–125 m).

The clay-marl layer is clearly prone to plastic behavior (Figure 8). The zones subject to traction are located in the surficial formations between the upstream chalk slabs. The active zone is subjected to shear and compression stresses.

4.2 Geophysical interpretations of the central profile

4.2.1. Electrical Resistivity Tomography (ERT)

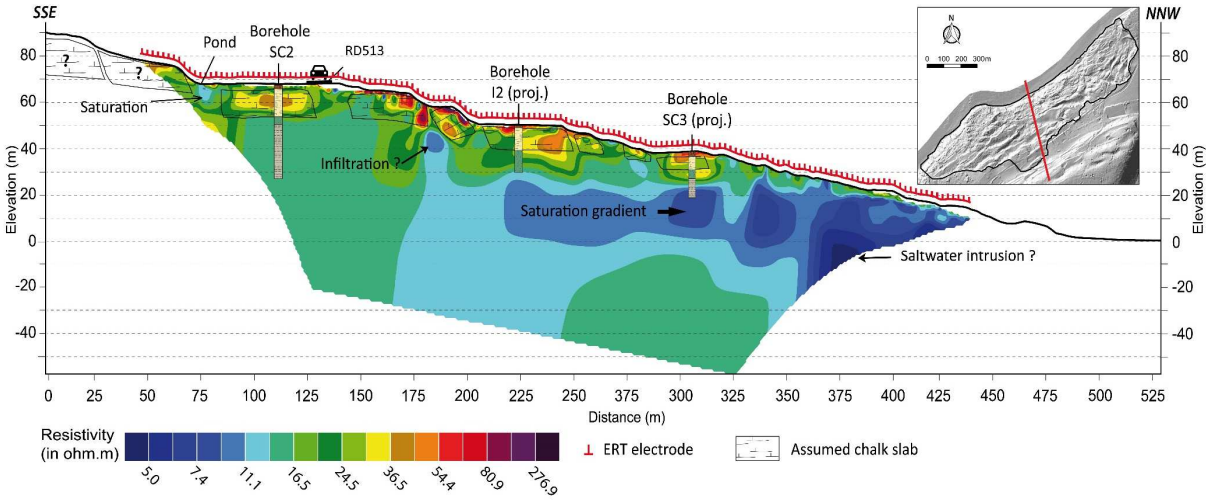

Figure 9- Results of the ERT profile inversion carried out in the central area of the Cirque des Graves.

The inversion was conducted with RES2DINV and indicates an absolute error of 3.66% after four iterations. The tomograms express low resistivities with values ranging between 3 and 100 Ω.m (Figure 9). Each class of value could be determined thanks to the three boreholes, SC2, I2 and SC3, located on or near the investigated profile, with identical altitude and morphological conditions. SC2 is located on the geophysical profile, and the other two boreholes, located at 60 and 80 m distances, are reprojected on the profile. From these empirical data, the extreme values (>100 Ω.m) are considered artifacts to be neglected in the interpretation. Chalk slabs are highlighted with the highest values, between 30 and 100 Ω.m, over thicknesses increasing upstream, from 4–5 m to a dozen meters at the top of the slope. Sand and clay are more complex to dissociate because they are in the same

value ranges, between 10 and 30 Ω.m. However, sands are slightly less conductive than clay and are instead in the range of 20–30 Ω.m.

A very weak resistivity anomaly (3–10 Ω.m) is visible downstream (in the interval X = 230–440 m), toward the foreshore, and attenuates upstream. This anomaly mainly occurs in the clays and marls at an altitude between 0 and 20 m NGF and extends into the calcareous sandstone bedrock downstream.

Finally, a few areas are barely more resistive at the surface (8–15 Ω.m), at the location of water accumulation areas (pond in the upstream and clay mudflows in the downstream) or at springs.

4.2.2. Seismic refraction

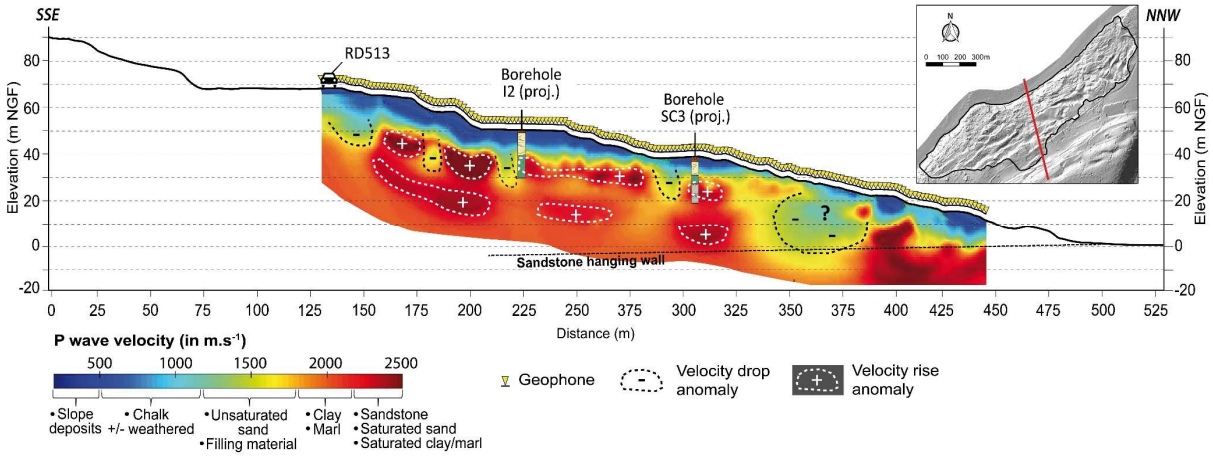

Figure 10- Results of the inversion of the seismic profile carried out in the central zone of the Cirque des Graves.

The seismic velocity is interpreted from the borehole logs of I2 (inclinometer) and SC3 (piezometer) (Figure 10). The surficial formations and chalk slabs show the lowest velocities near the surface, between 300 and 1200 m.s^{-1}.

Underneath the borehole logs, the velocities associated with the sands express a wide range of values, between 1200 and 2500 m.s^{-1}. Areas of extreme values (2200–2500 m.s^{-1}) appear in this formation two-thirds upstream of the profile. The strongest anomalies are localized at the top, at X=160–210 m.

A second layer of high-velocity anomalies is located at depth in the clayey-marl horizon, with similar values of approximately 2200–2500 m.s^{-1}. A significant but systematic decrease in velocity appears between these anomalies (1700–2000 m.s^{-1}). These lower velocities are continuous along the profile. Further down, the clayey marly materials are characterized by homogeneous velocities within the range of 1800–2200 m.s^{-1}.

In the downstream region (X=340–380 m), an anomaly of low speed is highlighted (1100–1600 $m.s^{-1}$). These velocities are theoretically related to sands and unsaturated surficial materials, which is not in accordance with field knowledge. This anomaly is explained by a lower coverage in seismic rays, the data containing noise from the sea (backwash) and dense vegetation (root suction).

Finally, the limit of the limestone is known because it crops out as bedrock, and the regional dip is known. It is affected by high velocities (2200–2500 $m.s^{-1}$) and is visible at the end of the profile. The concentric gradient generated by the low-velocity anomaly mentioned above partially hides it.

4.3. Interpretative cross-section of the central profile

The cross-analysis of geophysical surveys and in situ knowledge (geomorphology, geology, inclinometry, etc.) allows us to realize a geometric model in the center of the landslide. The boundary between the different layers and the variations in saturation are highlighted, as well as some velocity anomalies. The model proposed from these data is composed of nine chalk slabs of decreasing thickness downstream, including seven slabs in the unstable zone. The thickness of these slabs is heterogeneous and ranges from 5 m to 20 m, with a decreasing gradient from upstream to downstream.

The interpretative section in figure 11 summarizes all observations made from available data. This profile is then meshed into FLAC® to assess the stability and highlight the most likely slip surfaces.

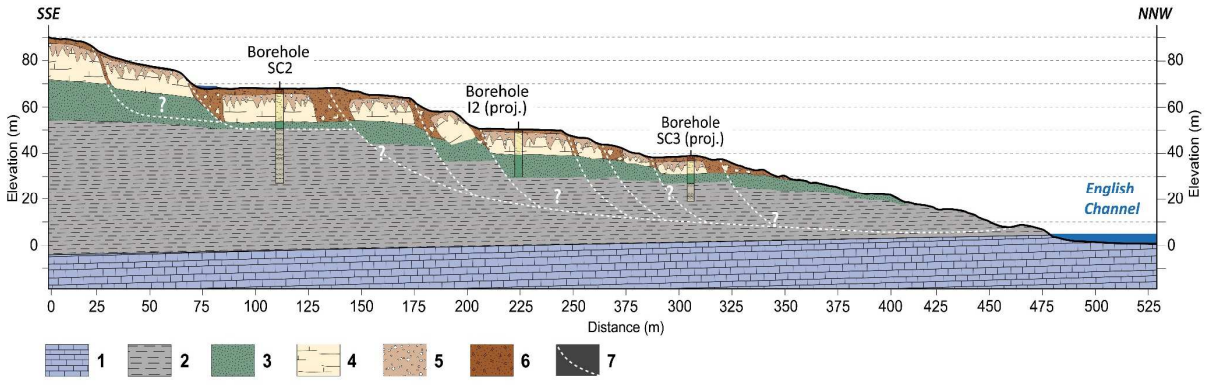

Figure 11- Interpretative cross-section in the center of the Cirque des Graves. Legend: 1. Hennequeville limestone, 2. Kimmeridgian and Oxfordian marls and clays, 3. Albian glauconitic sands, 4. Cenomanian chalk, 5. alteration products of the chalk, 6. Quaternary fill formations, and 7. different hypotheses of landslide surfaces.

441

442 **4.4 Hydromechanical modeling**

443 The mesh is shown in figure 12. The geomechanical parameters applied are those obtained from the back-
444 analysis in table 4.

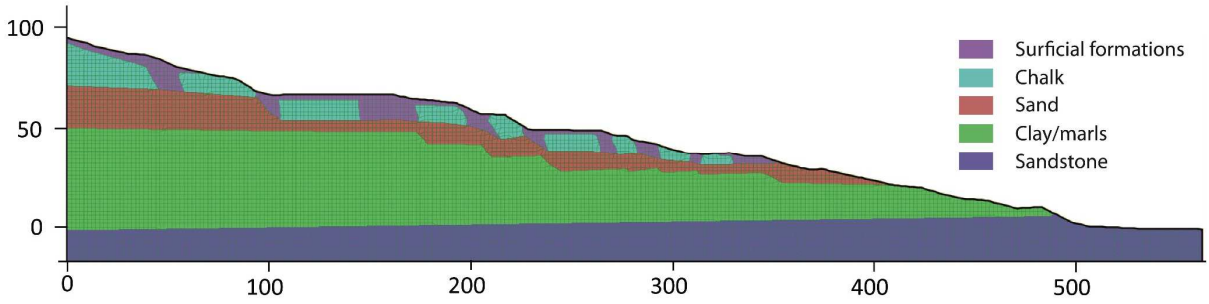

445

446 *Figure 12- Mesh created with FLAC® for the central profile of the Cirque des Graves.*

447 figure 13 shows the results for extremely high and low water. The numerical model extent was adjusted to the
448 length of the geometric model from geophysics for readability. Indeed, the modeled profile has a total length of
449 850 m, from the plateau to the sea.

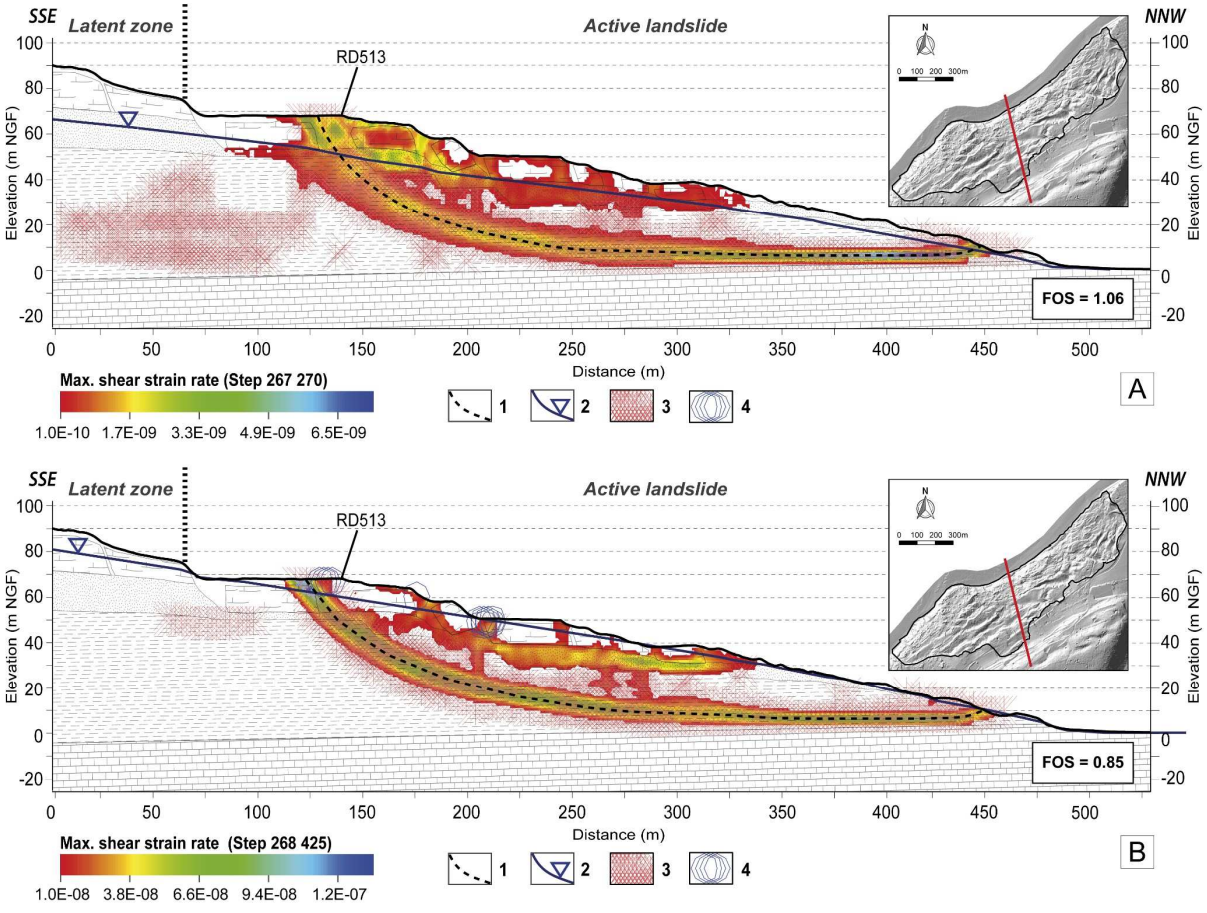

450

Figure 13- FLAC® results for the central profile and associated stress-strain (A) at low water for a level of 90 m NGF on the plateau and (B) at high water for a level of 116 m NGF on the plateau. Legend: (1) assumed slip surface from FLAC®; (2) piezometric level modeled under SEEP/W®; (3) nodes of the mesh exceeding the plasticity threshold in shear and compression; and (4) nodes of the mesh exceeding the plasticity threshold in tension.

The two scenarios at high and low water express similar results with regard to the calculated stresses, with some nuances. At high water, the assumed slip surface rises slightly higher in the marl (2 to 3 m) in the upstream part (X = 200 m). However, contact between the slip surface and sandstone substrate is at the same place (X = 350 m).

Several shear zones reach the surface at the main slope breaks and constitute secondary slip surfaces. At the surface, tensile stresses are calculated at high water and located near the three main sheared zones (X = 130, 175 and 210 m).

There is a concentration and a strong increase in the shear stress at high water, which occurs mainly along the deep slip surface and in the glauconitic sands located under the chalk. In the sands, the strongest deformation rates due to shear are located upstream at low water (Figure 13A) and downstream at high water (Figure 13B).

Uphill of RD513, there is no extension of the maximum shear strain rate under the chalk slab due to a deformation rate lower than the scale represented at high water. The deformation of this upstream zone is therefore not proportional to that experienced along the main slip surface. However, a number of nodes in the mesh exceed the plasticity criterion in the underlying sands, which is not the case at low water.

The low-water configuration shows that the model is already at the limit of stability, with a factor of safety of 1.06. The high-water model is widely above the instability threshold, with an estimated FoS of 0.85. The factor of safety quickly decreases below the unit as soon as the upstream water level on the plateau exceeds 93 m NGF (approximately -30 m). The bottom of the chalk aquifer is located regionally at approximately 78 m NGF.

5. Discussion

5.1. Toward a new structural model in the central zone

One of the challenges was to propose a geometric model of the center of the landslide. To do so, the prior empirical data (piezometry, inclinometry, and borehole logs) were crossed with geophysical data. Geophysics high-

lights the structure of the landslide and the presence of water and helps to confirm previous hypotheses regarding the functioning of the slope.

The ERT survey showed low resistivity values due to the nature of the materials (loose and weathered) and sometimes a high degree of saturation (Lissak et al., 2014a; Maquaire, 2000; Thirard et al., 2020). Very low resistivities due to saturation could be found at the pond located at the bottom of the main scarp at the upstream limit of the active zone (Figure 9). This observation is related to the discharge of plateau chalk groundwater (Thirard et al., 2020). The very low resistivity anomalies at the bottom of the slope can be linked to the increase in water content downstream and a growing salinity gradient due to marine intrusion and sea spray.

The coastal configuration of the landslide may induce the presence of a salted bevel at the foot of the slope. Sea water has a very low resistivity, on the order of 0.2 to 1 Ω.m (Jodry et al., 2014; Palacky, 1988). The drawdown observed in the limestone at approximately 100 m from the shoreline and characterized by values below 5 Ω.m seems to support this hypothesis. Clay is characterized by very low resistivities, which does not favor the appearance of strong contrasts in the lower layers (Skianis, 2012). However, it should be noted that a tidal influence was already observed in an old piezometer located approximately 80 m from the foot of the slope at the Fosses des Macres landslide, located in the neighboring municipality of Cricquebœuf. This site has a lithology and morphology similar to the Cirque des Graves. However, only additional investigations (piezometric, physicochemical and/or geochemical surveys) can confirm this assumption.

The seismic survey is consistent with ERT in terms of lithological interpretation. The ranges of values for each material category are broadly in agreement with the values obtained by previous studies (Lissak et al., 2014b) in the eastern part (Table 5).

Table 5- Comparison of seismic refraction results with values from Lissak et al. (2014b) in the eastern part of the Cirque des Graves.

Lithology	***Velocity (m.s) Lissak et al. (2014b)***	***Velocity (m.s) Current study (*saturated)***
Surficial formations (slope deposits, chalk-with-flints, etc.)	200–600	300–500
Chalk (more or less weathered)	600–1100	500–1200
Glauconitic sands (and surficial materials)	1100–1600	1200–1750 *(2300–2500*)*
Clay/Marl	1600–2200	1800–2200 *(2200–2500*)*
Sandstone	2200–2400	2200–2500

Low-velocity anomalies between chalk slabs fit unsaturated surficial materials. These anomalies are located at RD513 (assumed upstream limit of the main slip surface) but also at the bottom of secondary scarps. Between surficial materials and under the chalk slabs, Albian sands are defined by higher velocities, especially at the contact with clayey-marly materials. This can be attributed to the presence of a semicaptive water table but also to the settlement of these sands by sinking and readjustment of the Cenomanian chalk slabs. The increase in cohesion and induced saturation could explain these high velocities, between 2300 and 2500 m/s. Finally, the clayey marly facies has a high range of velocities, with an increase near 15 m below the sands (2200–2500 m/s), possibly explained by saturation within this layer.

This model based on seven chalk slabs is broadly in agreement with the morphostructural splitting of the site proposed by previous studies (Lissak, 2012; Lissak et al., 2014b). However, some discrepancies exist regarding slab width, initially estimated from discontinuous data on this portion of the landslide.

5.2. Slip surfaces and slope dynamics

The other aim of this work was to define assumed slip surfaces in the central profile that were not constrained by inclinometry, contrary to the calibration eastern profile. In the eastern profile, the back-analysis enabled us to simulate with precision the slip surface determined in situ (Figure 8) and to numerically reproduce the tilting-sinking of the chalk slabs in the underlying sands. These strong correlations with field knowledge allowed the transposition of geomechanical settings on the central profile. However, the shear zones modeled at the center of the landslide (Figure 13) must be compared with the geophysical data to validate the results of the numerical models.

The seismic refraction values show correlations with the slip surface simulated numerically with FLAC®. By juxtaposing the seismic anomalies (Figure 10) with the results of the numerical models (Figure 13), a correlation is highlighted between the deep shear and the high seismic velocity anomalies within the marl/clays (Figure 14). The continuity between the low-velocity anomaly near RD513 and the higher-velocity anomalies at depth suggest saturation of the clays along the slip surface, resulting in an increase in the measured velocities.

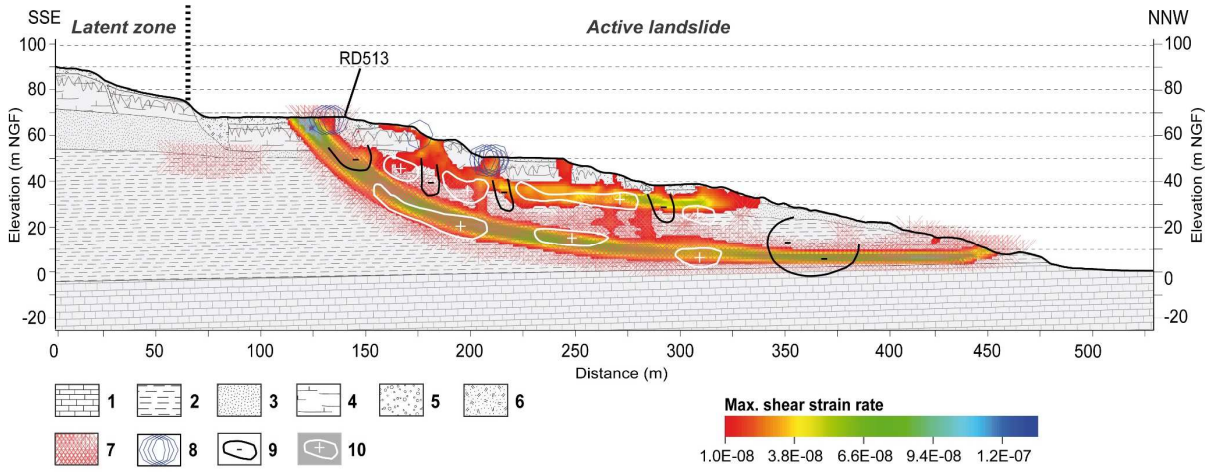

Figure 14- Correlations between seismic anomalies (Figure 10) and shear zones calculated with FLAC® at high water (Figure 13B). Legend: (1) limestone; (2) clay/marl; (3) sand; (4) chalk; (5) chalk alteration; (6) surficial and infill formations; (7) mesh nodes that exceeded the shear and compressional plasticity threshold; (8) mesh nodes that exceeded the tensile plasticity threshold; (9) low seismic velocity anomaly; and (10) high seismic velocity anomaly.

A decrease in the physical properties of the materials along a slip surface or into the surficial formations induces variations in P-wave velocity (Samyn et al., 2012). The increase or decrease in velocities directly relates to the water content, which depends on the seasonality and the inflow from the groundwater and impluvium (Grandjean et al., 2012; Malet, 2003). As the slip surface is located under the piezometric level, inflows possibly come from the upper horizons, including during low water periods, inducing permanent saturation. This assumption fits with previous results at the site, showing negative self-potential anomalies at the main scarp of this part of the landslide, indicating a downward movement of water, even at low water (Thirard et al., 2020). Based on this finding, it is likely that the low-velocity anomalies between chalk slabs and sands fit secondary slip surfaces along which water infiltrates to progressively moisten the clays and marls at depth.

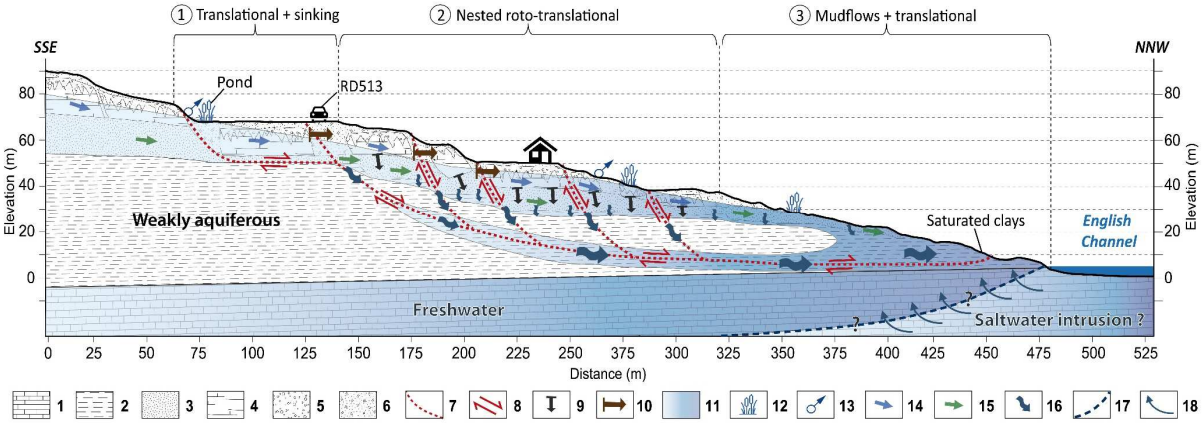

542

543 *Figure 15- Synthetic diagram of the hydromechanical behavior of the central profile of the Cirque des Graves. (1) Lime-*
544 *stone; (2) clay/marl; (3) sand; (4) chalk; (5) chalk alteration; (6) surficial formations; (7) highlighted slip surfaces; (8)*
545 *shear; (9) compression/compaction of sands; (10) main traction zones calculated with FLAC®; (11) aquifer or saturated*
546 *zone; (12) hygrophilic vegetation; (13) spring; (14) chalk water flow; (15) sand water flow; (16) clay wetting/infiltration*
547 *along slip surfaces; (17) freshwater/saltwater boundary; and (18) salt water pressure.*

548

549 In accordance with prior knowledge, the slope has the characteristics of a complex landslide with multiple nested
550 slip surfaces. The dynamics of the slope were broadly described as multiple rotational by Buma and Van Asch
551 (1996). Nevertheless, the translational component affecting the entire unstable zone and the flattening of the slip
552 surface at depth also suggest retrogressive multiple lateral spread (Hungr et al., 2014; Varnes, 1978). Finally,
553 chalk slabs are affected by the surficial dynamics of tilting and sinking into Albian sands. This dynamic coexists
554 with a deeper dynamic in clay marls, which is common in complex landslides (Guzzetti et al., 2004; Mergili et
555 al., 2014; Zêzere et al., 2005). In detail, the behavior can be divided into three subareas from upstream to down-
556 stream (Figure 15):

557 (1) The upstream part of RD513 has a translational dynamic related to the capability of the underlying
558 glauconitic sands to creep (Doré et al., 1987). This creeping coexists with a sinking of the slabs into the
559 sands. A DGPS benchmark located near SC2 and monitored several times a year (Figure 18) shows an
560 average subsidence rate of 2.7 $cm.yr^{-1}$ over the 2009–2020 period for a translational displacement of
561 7.1 $cm.yr^{-1}$ over the same period (Figure 18). However, the depth of the clay in borehole logs shows that
562 it is not impacted by the instability in this part of the slide. Therefore, it is probably not affected by a
563 deep slip surface but rather by a movement in contact with sands.

(2) Downstream of RD513 and up to the last downstream chalk slab, the dynamic is nested rotational-translational. The chalk slabs sink into the sands but are also subject to tilting by the reactivation of deep slip surfaces. It is noticeable in typical slope/counterslope morphology. Seismic data and numerical models suggest that the main slip surface extends to a 35 m depth in the middle of the cross-section. Inclinometer I2 and piezometer SC3, both 21 m deep and installed in 2005, have not yet been destroyed by the landslide in the past 15 years (Figure 11). Their integrity suggests deeper slip surfaces.

(3) Finally, from the last chalk slab onwards, translational dynamics predominate. It coexists with solifluction and mudflows due to the seepage of numerous springs at the outcrop of the sand groundwater (Thirard et al., 2020). Moreover, this area collects all upstream water inputs and seems globally saturated, although its clayey character provides, in theory, bad hydraulic conductivity.

5.3 Interest and limits of the back-analysis for the assessment of the hydromechanical behavior

5.3.1 Influence of water table levels on slope stability

The piezometric sensitivity analysis shows that the slope is already at the limit of stability at very low water levels (upstream water table at 90 m NGF), with a factor of safety of 1.06. For the exact setting transposition (Table 4), the limit equilibrium is computed for an upstream level barely higher than 93 m NGF (Figure 16), which remains low.

Above 93 m NGF, the model is unable to converge. FLAC® works by iterative calculations until an equilibrium state is reached. Thus, the calculation of FoS becomes impossible on an unstable slope. Under unstable conditions, the factor of safety was therefore approximated. The calculations were carried out on the basis of 50,000 iterations for the determination of the initial stress state in elastoplastic mode for all models presenting a numerical state of imbalance. The FoS was then estimated for the state corresponding to the last iteration calculated. By allowing sufficient time for the model to converge with the same number of iterations, the FoS can be approximated, and the results can be compared.

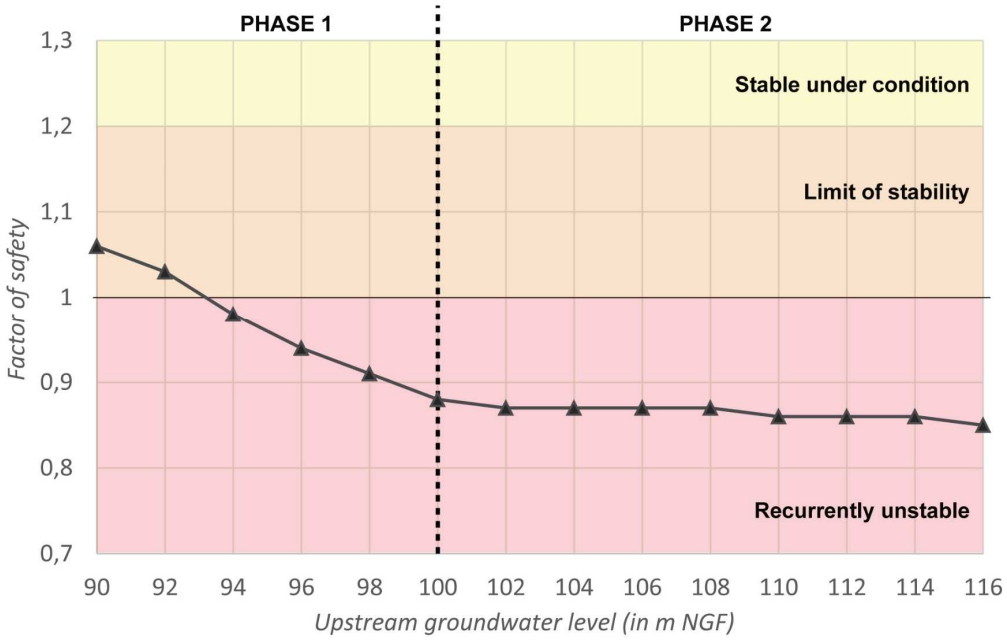

588

589 *Figure 16- Impact of the evolution of the upstream water table on the overall factor of safety of the slope.*

590 As the groundwater level rises, the FoS decreases in two different phases (Figure 16). In the first phase, a regular
591 decrease in FoS is observed from 90 to 100 m NGF. At 100 m, the FoS is already very low and reaches 0.88.
592 This level matches the saturation of the downstream part of the slope. Above 100 m, only the piezometric level
593 upstream of the model continues to grow significantly, which explains the lower impact on the overall calculated
594 FoS. Between 90 and 100 m NGF, the FoS decreases by approximately 2% per meter of groundwater rise, com-
595 pared with only 0.2% above 100 m NGF.

596 The overall impact of groundwater remains low with regard to the evolution of the factor of safety. However, as
597 the slope is always near the limit of stability, a small water overload can involve motion of the landslide. This
598 low stability raises questions and must be discussed in terms of kinematic functioning on the one hand and
599 methodological choices on the other.

600

601 ***5.3.2. Sensitivity analysis and limitations of the model***

602 The geomechanical setting and the transposition from the back-analysis parameters must be discussed with re-
603 spect to the results obtained. Theoretically, the lithological alternations are similar, and the materials have the
604 same properties between the center and eastern part of the landslide. However, it is possible that local structural
605 heterogeneities not integrated into the model result in a lower factor of safety in the central area. The low stabil-

606 ity may also be indicative of a very high geotechnical complexity, which is difficult to approximate by using
607 conventional modeling tools (Cambou et al., 2019).

608 The influence of cohesion and friction angle was theoretically assessed to determine the influence of the Mohr-
609 Coulomb parameters. This analysis was carried out for the clayey-marly layer, which is known to be responsible
610 for major displacements. Figure 17 shows the dependence of the factor of safety on C' and ϕ'. The tested value
611 ranges are in accordance with the geotechnical synthesis for weathered and sound clayey-marly materials (Table
612 1), i.e., from 0 to 100 kPa for C' and from 1 to 30° for ϕ'. The two parameters had independent sensitivity tests
613 for an upstream groundwater level at 100 m NGF (FoS = 0.88), corresponding to a near-saturated level of the
614 downstream part of the slope.

615

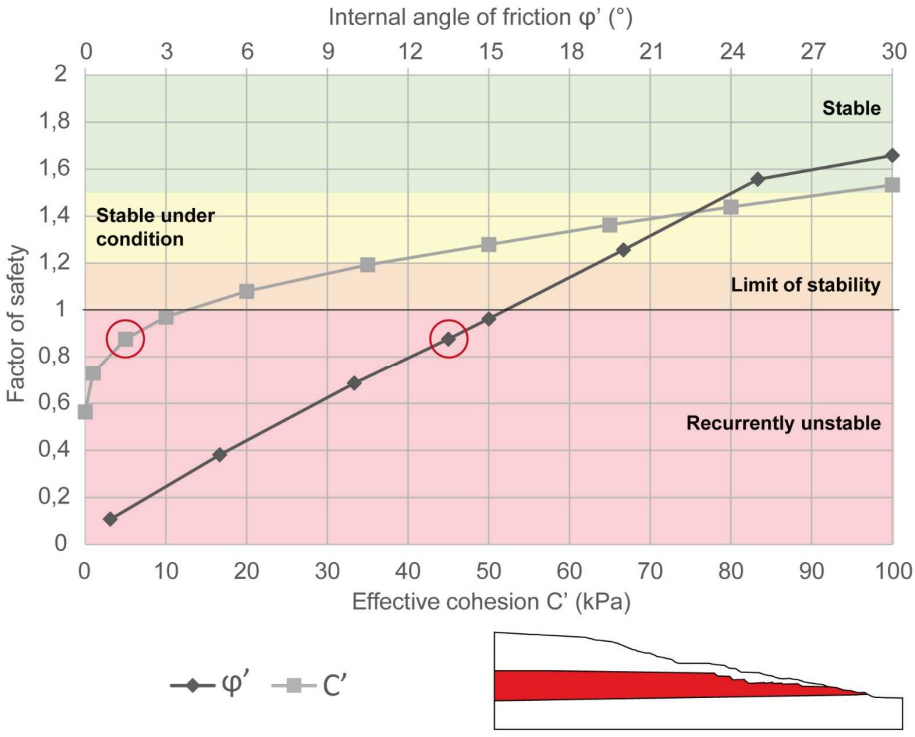

616

617 *Figure 17- Evolution of the global factor of safety of the central profile as a function of the variation of the cohesion and the*
618 *angle of friction of the clayey-marly materials. The values surrounded by a red circle relate to the transposition parameters*
619 *(C'=5 kPa; ϕ'=13.5°) for which FoS = 0.88. The lower abscissa is relative to the effective cohesion variation curve, and the*
620 *upper abscissa refers to the friction angle variation curve.*

621 Stability is very sensitive to these two parameters. Under downstream saturation conditions, the limit of stability
622 is reached for a friction angle of 15.5° with a cohesion of 5 kPa and for a cohesion of 12 kPa with a friction angle

of 13.5°. The lowering of cohesion leads to a linear decrease in the FoS, followed by a collapse for values lower than 20 kPa.

A small variation of the chosen parameters (i.e., C'=5 kPa; ϕ'=13.5°) is sufficient to make the slope totally stable or unstable. These tests also show the necessity to consider residual values, as cohesion and friction angle for sound materials induce a very high factor of safety. The only reinforcement of the clay-marl layer is sufficient to increase the FoS up to 1.5, which is in the unconditional stability domain.

As FLAC® uses a global method, these high stability values are questionable, whereas the cohesions considered in the sands and surficial formations are also very low (3 and 7 kPa, respectively). Although FLAC® manages to model the deformations around the chalk slabs, it has some difficulties in considering a realistic factor of safety for these layers. Indeed, it is well adapted to the analysis of continuous media but was not designed to model the complex dynamics shown at the near surface. Although the model enables the identification of strain zones within these layers, the numerical simulation of its stability is a limiting factor of this model.

5.4. A possible link between kinematics and pore water pressure

One possible explanation for the general low stability values is the kinematics of the slope. This landslide is in permanent motion and alternates between seasonal activity and exceptional outbursts (i.e., major reactivation). Continuous basic movement was measured, including during low water periods. This movement was attested by differential GPS surveys (Trimble 5700 GPS receiver and a Trimble R6 GNSS system) carried out on fixed concrete benchmarks distributed in the unstable zone (Lissak, 2012). Within this monitoring network, two benchmarks are located along the central profile and provide evidence of this continuous activity.

figure 18 shows higher speeds downstream of RD513 (B2) than upstream (B1). Between 2009 and 2020, B1 underwent a displacement of 81 cm (7 cm. yr^{-1}), compared with 190 cm at benchmark B2 (15 cm. yr^{-1}). Although the evenness of the surveys was not optimal over the survey period, it confirmed an activity even during the hydrological summer (i.e., low water period). For example, from May 25 to October 7, 2009, B1 underwent a translation of 2.7 cm and B2 underwent 3.0 cm. More recently, from March 27 to October 23, 2019, B1 shifted 2.1 cm and B2 shifted 2.6 cm. The average velocities were halved during the low water period, but the motion continued, showing that equilibrium was never reached.

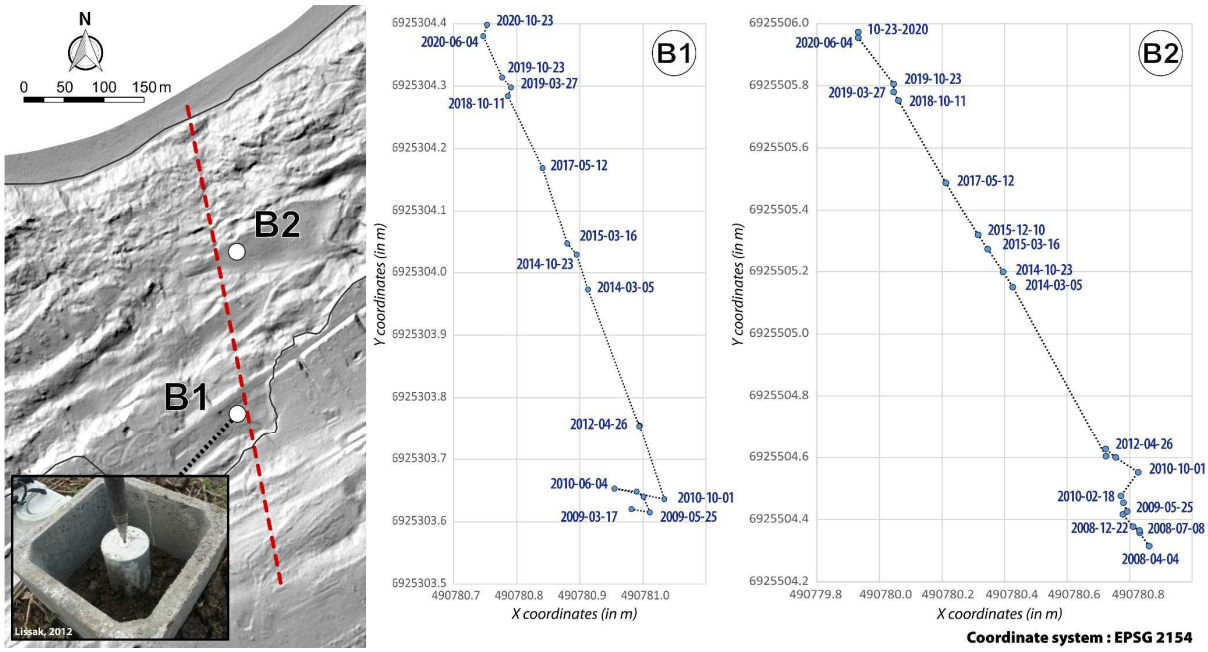

Figure 18- Displacements characterized by DGPS point tracking at benchmarks B1 and B2 along the central profile of the Cirque des Graves between 2008 and 2020.

Conversely, the eastern part of the landslide (Parc des Graves), which was modeled by back-analysis, experiences less pronounced seasonal shifts. In the summer period (i.e., low water), the displacements are barely perceptible and frequently within the GNSS error ellipse, which is on the order of a centimeter (Lissak, 2012). This area is also less affected by the water discharge from the plateau and experiences less vertical water inflows (Thirard et al., 2020). However, this eastern zone experienced greater movements during the major past events in 1982, 1988 and 2001 with significant infrastructure damage (Flageollet and Helluin, 1987; Lissak, 2012; Maquaire, 1990).

The determining role of pore pressures on the kinematics of landslides has been highlighted by many authors, as they strongly affect the balance of forces, especially in clay slides (Baum and Johnson, 1993; Bogaard et al., 2013; Bogaard and Greco, 2016; Malet et al., 2005; Van Asch et al., 1999). In particular, the major impact of saturation is known for cohesion (Matsushi and Matsukura, 2006). However, the collected data highlight a great heterogeneity of the slope saturation (Figure 15) related to erratic water circulation, as well as concentrated waterflow along discontinuities, especially along shear planes.

This refers to what Baum and Johnson (1993) called the forced circulation of pore water. The roughness along the slip surface affecting clayey slopes generates interstitial overpressures around the obstacles encountered. It tends to generate plasticity in materials located in the vicinity of the asperities of the slip surface.

Based on this, a more intense and deeper water circulation in the center of the landslide could induce a more frequent release of kinetic energy. This could lead to more regular readjustments due to this "forced circulation". The eastern part could experience more spaced loading/unloading stress cycles and thus a greater accumulation of stress, which results in more brutal movements.

Furthermore, prior studies have shown that landslides with continuous activity frequently return to stability values below unity (Malet et al., 2005; Maquaire et al., 2003). This could explain the lower factor of safety on the central profile than on the eastern calibration profile. However, it raises questions about the ability of conventional models to properly assess the stability of landslides with a "long-term/short-term" kinematic duality, characterized by continuous shifts and more sudden accelerations.

6. Conclusion

The aim of this study was to assess the hydromechanical functioning of a profile with stakes across a deep complex landslide. To do so, high-resolution 2D geophysics and finite difference modeling (FDM) were jointly used and showed consistent results.

FLAC® models were used to corroborate the assumptions based on geophysics and to validate these numerically. The challenge was to validate the results of numerical models on a profile where no slip surfaces or extreme water levels were known. To achieve relevant model settings, a back-analysis was performed on geomechanical parameters. The calibration was carried out in the eastern part of the landslide on a profile for which inclinometric and piezometric data were available.

On the central profile, geophysical data were cross-analyzed with empirical knowledge (boreholes, geomorphological knowledge, etc.) to propose a geometric model with five lithologies. Seismic and ERT surveys highlighted an uneven saturation of the slope and the possible presence of a saline wedge intrusion. This saturation is controlled not only by the intrinsic characteristics of the materials (hydraulic conductivity, porosity, etc. but also by discontinuities within the landslide (decompressed zones between chalk slabs and slip surfaces). These dis-

continuities allow saturating materials that are not very permeable in theory but behave like an aquitard by slowly filling up with water.

A breakdown of the landslide behavior was highlighted from upstream to downstream. Upstream of road RD513, the models and the survey results show a translational component with a shear surface in the sands at the contact with the clays. Slight subsidence is also highlighted due to the creep of the underlying sands. The major slip surface is located downstream of RD513 and propagates to the bottom of the slope until 35 m deep. This rupture is located within the clayey marly materials, as assumed from the seismic survey, and as evoked by prior studies. The presence of nested secondary slip surfaces with a roto-translational component is confirmed by the presence of shear strains and low seismic velocity anomalies between the chalk slabs. Finally, the bottom of the slope shows translational dynamics with surficial clay mudflows due to a major saturation from all upstream water inputs.

The combined contribution of geophysics and numerical modeling allowed us to converge on a robust functioning assumption. The implementation of inclinometric devices down to the bedrock would help to validate the simulated slip surfaces. Such devices at the bottom of the slope would also allow us to check the extent of the assumed salt bevel.

FLAC® appears to be a tool of interest for the assessment of slip surfaces and related stress-strain. However, it has some difficulties simulating the tilting and creep movements in the upper formations (sand, chalk, and surficial formations). Indeed, the software is not designed to analyze discontinuous media, which is a limitation of its use. The use of finite difference modeling associated with the classical Mohr-Coulomb criterion is not optimal for the stability analysis of a large slide with high lithological and kinematic complexity. To circumvent these problems, recent numerical developments show interest of second-order work in classical models incorporating discontinuity analysis, allowing us to better approximate the stability state of the slope (Cambou et al., 2019; Hu et al., 2020; Lignon et al., 2009). However, this method remains more expensive in terms of time and computing power, which complicates their implementation in an operational context.

The smoothed particle finite element method (SPFEM) could also be of interest to validate these results and is also the subject of recent advances. It handles the interfaces between particles and thus the interfaces between disjointed materials. It allows us to understand the spatial and temporal decoupling of the dynamics of complex retrogressive landslides undergoing large deformations (Jin et al., 2020; Yuan et al., 2020; Zhang et al., 2021).

Acknowledgements

This research was supported by the ANR RICOCHET project: "Multi-risk assessment of coastal territories in a context of global change (2017-2021)" (Grant number: ANR-16-CE03-0008), funded by the French National Research Agency (ANR).

The Villerville landslide, locally managed by LETG-Caen laboratory, is a permanent site instrumented as part of the OMIV-INSU observatory (French Observatory on Landslides) led by the EOST laboratory at the University of Strasbourg.

The authors thank all the people involved in the field surveys within the LETG-Caen and BRGM teams, in particular Robert Davidson, Augustin Sallent and Mickael Delatre. We also express our gratitude to the members of the GdRI GeoMech (International research network in Geo-environmental Mechanics) for the valuable discussions regarding the interpretations and limits of the numerical models, particularly Pierre-Yves Hicher, Félix Darve, Luc Closset and François Nicot.

737 **Bibliographie**

738 Alonso, E.E., Pinyol, N.M., 2015. Slope stability in slightly fissured claystones and marls. Land-
739 slides 12, 643–656.
740 Arthur, J., Dunstan, T., Al-Ani, Q., Assadi, A., 1977. Plastic deformation and failure in granular
741 media. Geotechnique 27, 53–74.
742 Baum, R.L., Johnson, A.M., 1993. Steady movement of landslides in fine-grained soils: A model for
743 sliding over an irregular slip surface. US Government Printing Office.
744 Bergin, J.-P., 1972a. Trapil. Oléoduc pont-Jerome-Caen. Communes de Grangues, Périers-en-Auge
745 et Varaville (Calvados). Reconnaissances géotechniques ponctuelles. Compte-rendu
746 d'essais. 10 p. BRGM/72-SGN-215-NPA.
747 Bergin, J.-P., 1972b. Trapil. Oléoduc port-Jerome-Caen. Communes de saint-Gatien-des-bois et de
748 Saint-Martin-aux-Chartrains (calvados). Reconnaissances géotechniques ponctuelles.
749 Compte-rendu d'essais, 11 p. 1 pht.
750 Berthaud, Y., de Buhan, P., Schmitt, N., 2018. Aide-mémoire-Mécanique des sols-3e éd.: Aspects
751 mécaniques des sols et des structures. Dunod.
752 Bitri, A., Perrin, J., Beauce, A., 1996. La sismique réflexion haute résolution : principes et applica-
753 tions. Rapport BRGM R 39220, 59p.
754 Bogaard, T., Maharjan, L.D., Maquaire, O., Lissak, C., Malet, J.-P., 2013. Identification of Hydro-
755 Meteorological Triggers for Villerville Coastal Landslide, in: Margottini, C., Canuti, P., Sas-
756 sa, K. (Eds.), Landslide Science and Practice. Springer Berlin Heidelberg, Berlin, Heidel-
757 berg, pp. 141–145. https://doi.org/10.1007/978-3-642-31427-8_18
758 Bogaard, T.A., Greco, R., 2016. Landslide hydrology: from hydrology to pore pressure. Wiley In-
759 terdisciplinary Reviews: Water 3, 439–459.
760 Brideau, M.-A., Stead, D., Couture, R., 2006. Structural and engineering geology of the East Gate
761 Landslide, Purcell Mountains, British Columbia, Canada. Engineering Geology 84, 183–
762 206. https://doi.org/10.1016/j.enggeo.2006.01.004

763 Buma, J., Van Asch, T., 1996. Slide (rotational). in Dikau, R., Brunsden, D., Schrott, L., Ibsen. ML
764 (eds.), Landslide Recognition, Identification, Movement and Causes. Great Britain, John
765 Wiley and Sons 43–61.
766 Cambou, B., Darve, F., Nicot, F., 2019. Particle methods in geomechanics. International Journal for
767 Numerical and Analytical Methods in Geomechanics 43, 831–832.
768 https://doi.org/10.1002/nag.2919
769 Caris, J., Van Asch, T.W., 1991. Geophysical, geotechnical and hydrological investigations of a
770 small landslide in the French Alps. Engineering Geology 31, 249–276.
771 Carlier, B., Carlier, G., Gance, J., Provost, F., Lissak, C., Graff, K., Viel, V., Arnaud-Fassetta, G., Fort,
772 M., Betard, F., 2018. Distribution spatiale et estimation des volumes sédimentaires dans
773 un bassin-versant de schistes lustrés: l'exemple du Peynin (Queyras, Alpes du Sud).
774 Géomorphologie: relief, processus, environnement 24, 59–76.
775 Cebulski, J., Pasierb, B., Wieczorek, D., Zieliński, A., 2020. Reconstruction of landslide movements
776 using Digital Elevation Model and Electrical Resistivity Tomography analysis in the
777 Polish Outer Carpathians. CATENA 195, 104758.
778 https://doi.org/10.1016/j.catena.2020.104758
779 CETE, 1978. Villerville : stabilité de la digue en enrochement. Labo Rég. P. et Ch. de Rouen, Af-
780 faire n°9129/1, 5 janv., 50 p.
781 Chen, H.J., Yuan, W.B., 2012. Application of FLAC to Study on Anchorage for Mountain Slope. AMR
782 535–537, 1944–1949. https://doi.org/10.4028/www.scientific.net/AMR.535-537.1944
783 Chen, Q., Zhang, S., Chang, S., Liu, B., Liu, J., Long, J., 2019. Geophysical Interpretation of a Subsur-
784 face Landslide in the Southern Qinshui Basin. Journal of Environmental and Engineering
785 Geophysics 18.
786 Coulouma, G., Samyn, K., Grandjean, G., Follain, S., Lagacherie, P., 2012. Combining seismic and
787 electric methods for predicting bedrock depth along a Mediterranean soil toposequence.
788 Geoderma 170, 39–47. https://doi.org/10.1016/j.geoderma.2011.11.015

789 Cundall, P., Coetzee, M., Hart, R., Varona, P., 1993. FLAC user's manual. Itasca Consulting Group,
790 USA.
791 Dawson, E.M., Roth, W.H., Drescher, A., 1999. Slope stability analysis by strength reduction. Géo-
792 technique 49, 835–840. https://doi.org/10.1680/geot.1999.49.6.835
793 Deiana, M., Mussi, M., Pennisi, M., Boccolari, M., Corsini, A., Ronchetti, F., 2020. Contribution of
794 water geochemistry and isotopes (δ18O, δ2H, 3H, 87Sr/86Sr and δ11B) to the study of
795 groundwater flow properties and underlying bedrock structures of a deep landslide. En-
796 viron Earth Sci 79, 30. https://doi.org/10.1007/s12665-019-8772-4
797 Denchik, N., Gautier, S., Dupuy, M., Batiot-Guilhe, C., Lopez, M., Léonardi, V., Geeraert, M., Henry,
798 G., Neyens, D., Coudray, P., Pezard, P.A., 2019. In-situ geophysical and hydro-geochemical
799 monitoring to infer landslide dynamics (Pégairolles-de-l'Escalette landslide, France). En-
800 gineering Geology 254, 102–112. https://doi.org/10.1016/j.enggeo.2019.04.009
801 Deschamps, R., Yankey, G., 2006. Limitations in the Back-Analysis of Strength from Failures. J.
802 Geotech. Geoenviron. Eng. 132, 532–536. https://doi.org/10.1061/(ASCE)1090-
803 0241(2006)132:4(532)
804 Doré, F., Juignet, P., Larsonneur, C., Pareyn, C., Rioult, M., 1987. Guide géologique régional 'Nor-
805 mandie-Maine'. Editions Masson, Paris. 216p.
806 Dugué, O., 1991. Comportement d'une bordure de massifs anciens et cortèges de minéraux argi-
807 leux: l'exemple de la bordure occidentale du Bassin Anglo-Parisien au Callovo-Oxfordien
808 24.
809 Duncan, J.M., 1996. State of the art: limit equilibrium and finite-element analysis of slopes. Jour-
810 nal of Geotechnical engineering 122, 577–596.
811 Elhaï, H., 1963. La Normandie occidentale entre la Seine et le golfe normand-breton. Etude mor-
812 phologique (Thèse d'Etat). Université de Paris, imprimerie Bière, Bordeaux.
813 Evrard, H., Sinelle, C., 1980. Stabilité des falaises du Pays de Caux. CETE, LRPC, Le Grand Quevilly
814 85 p.

Flageollet, J., Helluin, E., 1987. Morphological investigations in the sliding areas along coast of Pays d'Auge, near Villerville, Normandy, France. International Geomorphology 1, 447–486.

Flageollet, J., Helluin, E., 1984. Formations quaternaires et zonage des risques de glissements de terrain à Villerville et à Cricquebœuf (Calvados). Documents-BRGM 173–183.

Flageollet, J.-C., 1992. Quaternary slope formations between Trouville and Honfleur In: Flageollet, J.-C. (Ed.), Proceedings of the European Intensive Course on the Prevention of Coastal Erosion and Submersion Risks, CERG, Council of Europe, Major Hazards Agreement, Strasbourg, 9 p. 9.

Floris, M., Bozzano, F., 2008. Evaluation of landslide reactivation: a modified rainfall threshold model based on historical records of rainfall and landslides. Geomorphology 94, 40–57.

Fressard, M., 2013. Les glissements de terrain du Pays d'Auge continental (Normandie, France) Caractérisation, cartographie, analyse spatiale et modélisation (Thèse de géographie). Université de Caen.

Gance, J., 2014. Développements méthodologiques en géophysique haute résolution pour la caractérisation hydro-mécanique de glissements de terrain argileux.

Gance, J., Grandjean, G., Samyn, K., Malet, J.-P., 2012. Quasi-Newton inversion of seismic first arrivals using source finite bandwidth assumption: Application to subsurface characterization of landslides. Journal of Applied Geophysics 87, 94–106. https://doi.org/10.1016/j.jappgeo.2012.09.008

Gilli, E., Mangan, C., Mudry, J., 2008. Hydrogéologie-2ème édition-Objets, méthodes, applications: Objets, méthodes, applications. Dunod.

Grandjean, G., Bitri, A., Krzeminska, D.M., 2012. Characterisation of a landslide fissure pattern by integrating seismic azimuth tomography and geotechnical testing. Hydrological Processes 26, 2120–2127. https://doi.org/10.1002/hyp.7993

Grandjean, G., Pennetier, C., Bitri, A., Meric, O., Malet, J.-P., 2006. Caractérisation de la structure interne et de l'état hydrique de glissements argilo-marneux par tomographie géophy-

842 sique : l'exemple du glissement-coulée de Super-Sauze (Alpes du Sud, France). Comptes
843 Rendus Geoscience 338, 587–595. https://doi.org/10.1016/j.crte.2006.03.013
844 Guzzetti, F., Cardinali, M., Reichenbach, P., Cipolla, F., Sebastiani, C., Galli, M., Salvati, P., 2004.
845 Landslides triggered by the 23 November 2000 rainfall event in the Imperia Province,
846 Western Liguria, Italy. Engineering Geology 73, 229–245.
847 Hu, J., Li, Z., Darve, F., Feng, J., 2020. Advantages of second-order work as a rational safety factor
848 and stability analysis of a reinforced rock slope. Canadian Geotechnical Journal 57, 661–
849 672.
850 Hungr, O., Leroueil, S., Picarelli, L., 2014. The Varnes classification of landslide types, an update.
851 Landslides 11, 167–194.
852 Hürlimann, M., 2000. Back analysis of Swiss debris flows events, Description of the results ob-
853 tained from the FLO-2D simulations carried out during 2000. Report of Swiss Federal In-
854 stitute WSL, Water Soil and Rock Movements 2–14.
855 Hutchinson, J.N., Somerville, S.H., Petley, D.J., 1973. A landslide in periglacially disturbed Etruria
856 Marl at Bury Hill, Staffordshire. Quarterly Journal of Engineering Geology and Hydroge-
857 ology 6, 377–404. https://doi.org/10.1144/GSL.QJEG.1973.006.03.16
858 Hydrogeotechnique, 2007. Commune de Villerville - Confortement de la falaise, Villerville (14).
859 Rapport d'étude geotechnique. Missions G11-G12. (No. Dossier C/ME/06/L/385/L/137).
860 Hydrogeotechnique, 2006a. Communauté de communes cœur côte fleurie, Calvados (14) - Trou-
861 ville-sur-Mer. Lutte contre les mouvements de terrain, RD513, site du Chant des Oiseaux.
862 Rapport d'étude géotechnique, Mission G11. (No. Dossier C/ME/05/E/074/F/039).
863 Hydrogeotechnique, 2006b. Communauté de communes cœur côte fleurie, Calvados (14) - Vil-
864 lerville. Lutte contre les mouvements de terrain, RD513, Licorne-Trescartes. Rapport
865 d'étude géotechnique, Mission G0. (No. Dossier C/ME/05/E/074/F/039).
866 IMSRN, 2005. Création d'une station d'épuration sur la commune de Cricqueboeuf. Etude géo-
867 technique G0-G11, 12 p. + annexes.
868 Itasca, 2019. FLAC 8.0 User's Guide, Itasca Consulting Group. Inc. Minneapolis, USA.

869 Jin, Y.-F., Yin, Z.-Y., Yuan, W.-H., 2020. Simulating retrogressive slope failure using two different
870 smoothed particle finite element methods: A comparative study. Engineering Geology
871 279, 105870.
872 Jodry, C., Palma Lopes, S., Joubert, A., Sanchez, M., Côte, P., 2014. Suivi géoélectrique des intru-
873 sions d'eau salée sous un cordon dunaire côtier au cours d'une marée, in: XIIIèmes
874 JNGCGC Dunkerque. Presented at the Journées Nationales Génie Côtier - Génie Civil, Edi-
875 tions Paralia, pp. 591–600. https://doi.org/10.5150/jngcgc.2014.065
876 Jongmans, D., Garambois, S., 2007. Geophysical investigation of landslides : a review. Bulletin de
877 la Societe Geologique de France 178, 101–112.
878 https://doi.org/10.2113/gssgfbull.178.2.101
879 Journaux, A., 1971. Formations superficielles et dynamique des versants dans le pays d'Auge.
880 Presented at the Colloque International de Géomorphologie, Réunion de la commission
881 d'études des formations superficielles et de la dynamique des versants du Comité Natio-
882 nal de Géographie, Excursion dans le Pays d'Auge, p. 27.
883 Krabbenhøft, K., Lyamin, A.V., Sloan, S.W., 2008. Three-dimensional Mohr–Coulomb limit analy-
884 sis using semidefinite programming. Communications in Numerical Methods in Engi-
885 neering 24, 1107–1119.
886 Krahn, J., 2004. Seepage modeling with SEEP/W: An engineering methodology. GEO-SLOPE In-
887 ternational Ltd. Calgary, Alberta, Canada.
888 Li, L., Wang, Y., 2020. Identification of failure slip surfaces for landslide risk assessment using
889 smoothed particle hydrodynamics. Georisk: Assessment and Management of Risk for En-
890 gineered Systems and Geohazards 14, 91–111.
891 https://doi.org/10.1080/17499518.2019.1602877
892 Lignon, S., Laouafa, F., Prunier, F., Khoa, H., Darve, F., 2009. Hydro-mechanical modelling of land-
893 slides with a material instability criterion. Geotechnique 59, 513–524.

Lissak, C., 2012. Les glissements de terrain des versants côtiers du Pays d'Auge (Calvados) : Morphologie, fonctionnement et gestion du risque. (Thèse de géographie). Université de Caen, Caen, France.

Lissak, C., Maquaire, O., Davidson, R., Malet, J.-P., 2014a. Piezometric thresholds for triggering landslides along the Normandy coast, France. Geomorphologie 20, 145–158. https://doi.org/10.4000/geomorphologie.10607

Lissak, C., Maquaire, O., Malet, J.-P., Bitri, A., Samyn, K., Grandjean, G., Bourdeau, C., Reiffsteck, P., Davidson, R., 2014b. Airborne and ground-based data sources for characterizing the morpho-structure of a coastal landslide. Geomorphology 217, 140–151. https://doi.org/10.1016/j.geomorph.2014.04.019

Liu, S., Su, Z., Li, M., Shao, L., 2020. Slope stability analysis using elastic finite element stress fields. Engineering Geology 273, 13p. https://doi.org/10.1016/j.enggeo.2020.105673

Loke, M., 1999. A practical guide to 2D and 3D surveys. Electrical imaging surveys for environmental and engineering studies. A Practical Guide to 2-D and 3-D Surveys.

Loke, M.H., Acworth, I., Dahlin, T., 2003. A comparison of smooth and blocky inversion methods in 2D electrical imaging surveys. Exploration Geophysics 34, 6.

Loke, M.H., Barker, R.D., 1996. Rapid least-squares inversion of apparent resistivity pseudosections by a quasi-Newton method1. Geophys Prospect 44, 131–152. https://doi.org/10.1111/j.1365-2478.1996.tb00142.x

Lollino, P., Cotecchia, F., Elia, G., Mitaritonna, G., Santaloia, F., 2014. Interpretation of landslide mechanisms based on numerical modelling: two case-histories. null 20, 1032–1053. https://doi.org/10.1080/19648189.2014.985851

Lu, C.-Y., Tang, C.-L., Chan, Y.-C., Hu, J.-C., Chi, C.-C., 2014. Forecasting landslide hazard by the 3D discrete element method: A case study of the unstable slope in the Lushan hot spring district, central Taiwan. Engineering Geology 183, 14–30.

Malamud, B.D., Turcotte, D.L., Guzzetti, F., Reichenbach, P., 2004. Landslide inventories and their statistical properties. Earth Surf. Process. Landforms 29, 687–711. https://doi.org/10.1002/esp.1064

Malet, J.-P., 2003. Les 'glissements de type écoulement' dans les marnes noires des Alpes du Sud. Morphologie, fonctionnement et modélisation hydro-mécanique (Thèse de doctorat). Université Louis Pasteur-Strasbourg I.

Malet, J.-P., van Asch, Th.W.J., van Beek, R., Maquaire, O., 2005. Forecasting the behaviour of complex landslides with a spatially distributed hydrological model. Nat. Hazards Earth Syst. Sci. 5, 71–85. https://doi.org/10.5194/nhess-5-71-2005

Maquaire, O., 2000. Effects of groundwater on the Villerville-Cricqueboeuf landslides. Sixteen years of survey (Calvados, France). Presented at the 8th Landslides International symposium, Cardiff, pp. 1005–1010.

Maquaire, O., 1990. Les mouvements de terrain de la côte du Calvados: recherche et prévention. Editions du BRGM, vol. 197.

Maquaire, O., Gigot, P., 1988. Reconnaissance par sismique réfraction de la décompression et de l'instabilite des falaises vives du Bessin (Normandie, France). Geodinamica Acta 2, 151–159. https://doi.org/10.1080/09853111.1988.11105163

Maquaire, O., Malet, J.-P., Remaıtre, A., Locat, J., Klotz, S., Guillon, J., 2003. Instability conditions of marly hillslopes: towards landsliding or gullying? The case of the Barcelonnette Basin, South East France. Engineering geology 70, 109–130.

Matsushi, Y., Matsukura, Y., 2006. Cohesion of unsaturated residual soils as a function of volumetric water content. Bull Eng Geol Environ 65, 449. https://doi.org/10.1007/s10064-005-0035-9

Mergili, M., Marchesini, I., Rossi, M., Guzzetti, F., Fellin, W., 2014. Spatially distributed three-dimensional slope stability modelling in a raster GIS. Geomorphology 206, 178–195. https://doi.org/10.1016/j.geomorph.2013.10.008

945 Meric, O., Garambois, S., Jongmans, D., Wathelet, M., Chatelain, J.L., Vengeon, J.M., 2005. Applica-
946 tion of geophysical methods for the investigation of the large gravitational mass move-
947 ment of Séchilienne, France. Can. Geotech. J. 42, 1105–1115.
948 https://doi.org/10.1139/t05-034
949 Michalowski, R.L., 2002. Stability Charts for Uniform Slopes. J. Geotech. Geoenviron. Eng. 128,
950 351–355. https://doi.org/10.1061/(ASCE)1090-0241(2002)128:4(351)
951 Palacky, G., 1988. Resistivity characteristics of geologic targets. Electromagnetic methods in ap-
952 plied geophysics 1, 53–129.
953 Pareyn, C., Voiment, R., Dabissat, C., 1982. Le glissement de Villerville (Calvados) de janvier
954 1982 : Modalités, causes probables, perspectives d'évolution. Rapport préliminaire, 10
955 février 1982, 16 p.
956 Pasierb, B., Grodecki, M., Gwóźdź, R., 2019. Geophysical and geotechnical approach to a landslide
957 stability assessment: a case study. Acta Geophys. 67, 1823–1834.
958 https://doi.org/10.1007/s11600-019-00338-7
959 Pazzi, V., Morelli, S., Fanti, R., 2019. A Review of the Advantages and Limitations of Geophysical
960 Investigations in Landslide Studies. International Journal of Geophysics 2019, 1–27.
961 https://doi.org/10.1155/2019/2983087
962 Perrone, A., Lapenna, V., Piscitelli, S., 2014. Electrical resistivity tomography technique for land-
963 slide investigation: A review. Earth-Science Reviews 135, 65–82.
964 https://doi.org/10.1016/j.earscirev.2014.04.002
965 Plumelle, C., Cui, Y.J., Fabre, D., Fouché-Grobla, O., Hirschauer, A., Tabbagh, A., Briançon, L., Gourc,
966 J.-P., 2013. Théorie et pratique de la géotechnique: Exercices et applications de méca-
967 nique des sols. Éditions" Le Moniteur.
968 Prunet, F., 2001. Glissements de terrains à Trouville-sur-Mer. Note de synthèse. (No. Dossier
969 01779).
970 Rice, J., 1976. The localization of plastic deformation, w: Theoretical and applied mechanics, red.
971 WT Koiter. North-Holand 207, 220.

Samyn, K., Travelletti, J., Bitri, A., Grandjean, G., Malet, J.-P., 2012. Characterization of a landslide geometry using 3D seismic refraction traveltime tomography: The La Valette landslide case history. Journal of Applied Geophysics 86, 120–132.

Shen, H., Klapperich, H., Abbas, S.M., Ibrahim, A., 2012. Slope stability analysis based on the integration of GIS and numerical simulation. Automation in Construction 26, 46–53. https://doi.org/10.1016/j.autcon.2012.04.016

Shi, W., Li, Y., Zhang, W., Liu, J., He, S., Mo, P., Guan, F., 2020. The loess landslide on 15 march 2019 in Shanxi Province, China. Landslides 17, 677–686. https://doi.org/10.1007/s10346-019-01342-0

Skianis, G.A., 2012. The Self-Potential Anomaly Produced by a Subsurface Flow at the Contact of Two Horizontal Layers and Its Quantitative Interpretation. International Journal of Geophysics 1–8.

Tang, C.-L., Hu, J.-C., Lin, M.-L., Angelier, J., Lu, C.-Y., Chan, Y.-C., Chu, H.-T., 2009. The Tsaoling landslide triggered by the Chi-Chi earthquake, Taiwan: insights from a discrete element simulation. Engineering Geology 106, 1–19.

Tang, W.H., Stark, T.D., Angulo, M., 1999. Reliability in back analysis of slope failures. Soils and Foundations 39, 73–80.

Thirard, G., Grandjean, G., Thiery, Y., Maquaire, O., François, B., Lissak, C., Costa, S., 2020. Hydrogeological assessment of a deep-seated coastal landslide based on a multi-disciplinary approach. Geomorphology 371, 107440. https://doi.org/10.1016/j.geomorph.2020.107440

Touitou, D., 2002. Apport de la modélisation et de l'instrumentation dans l'analyse de la stabilité et de la déformation à long terme d'un massif granitique: Application aux talus de grande hauteur de l'écluse à bateaux permanente au barrage des Trois Gorges (Chine). PhD thesis, 432 p. (PhD thesis). Ecole des Ponts ParisTech.

997 Travelletti, J., 2011. Imagerie multi-paramètres et multi-résolutions pour l'observation et la ca-
998 ractérisation des mécanismes de glissements-coulées, PhD thesis, University of Caen-
999 Normandie. 323 p.
1000 Unisol, 2009. Glissement de terrain, 8 rue du Littoral 14113 Villerville (Mission G5). (Diagnostic
1001 géotechnique No. Dossier 09101020).
1002 Van Asch, Th.W.J., Buma, J., Van Beek, L.P.H., 1999. A view on some hydrological triggering sys-
1003 tems in landslides. Geomorphology 30, 25–32. https://doi.org/10.1016/S0169-
1004 555X(99)00042-2
1005 van Asch, T.W.J., Malet, J.-P., van Beek, L.P.H., Amitrano, D., 2007. Techniques, issues and advanc-
1006 es in numerical modelling of landslide hazard. Bulletin de la Société Géologique de
1007 France 178, 65–88. https://doi.org/10.2113/gssgfbull.178.2.65
1008 Van Den Eeckhaut, M., Moeyersons, J., Nyssen, J., Abraha, A., Poesen, J., Haile, M., Deckers, J., 2009.
1009 Spatial patterns of old, deep-seated landslides: A case-study in the northern Ethiopian
1010 highlands. Geomorphology 105, 239–252.
1011 Van Den Eeckhaut, M., Verstraeten, G., Poesen, J., 2007. Morphology and internal structure of a
1012 dormant landslide in a hilly area: The Collinabos landslide (Belgium). Geomorphology
1013 89, 258–273. https://doi.org/10.1016/j.geomorph.2006.12.005
1014 Varnes, D.J., 1978. Slope movement types and processes. Special report, National Academy of
1015 Sciences 176, 11–33.
1016 Whiteley, J.S., Chambers, J.E., Uhlemann, S., Wilkinson, P.B., Kendall, J.M., 2019. Geophysical Mon-
1017 itoring of Moisture-Induced Landslides: A Review. Rev. Geophys. 57, 106–145.
1018 https://doi.org/10.1029/2018RG000603
1019 Xu, B., Yan, C., Lu, Q., He, D., 2014. Stability assessment of Jinlong village landslide, Sichuan. Envi-
1020 ron Earth Sci 71, 3049–3061. https://doi.org/10.1007/s12665-013-2682-7
1021 Yuan, W.-H., Liu, K., Zhang, W., Dai, B., Wang, Y., 2020. Dynamic modeling of large deformation
1022 slope failure using smoothed particle finite element method. Landslides 1–13.

Zêzere, J.L., Trigo, R.M., Trigo, I.F., 2005. Shallow and deep landslides induced by rainfall in the Lisbon region (Portugal): assessment of relationships with the North Atlantic Oscillation. Natural Hazards and Earth System Sciences 5, 331–344.

Zhang, K., Cao, P., Bao, R., 2013. Rigorous back analysis of shear strength parameters of landslide slip. Transactions of Nonferrous Metals Society of China 23, 1459–1464. https://doi.org/10.1016/S1003-6326(13)62617-5

Zhang, W., Zhong, Z., Peng, C., Yuan, W., Wu, W., 2021. GPU-accelerated smoothed particle finite element method for large deformation analysis in geomechanics. Computers and Geotechnics 129, 103856.

Zhang, Z., Wang, T., Wu, S., Tang, H., Liang, C., 2017. The role of seismic triggering in a deep-seated mudstone landslide, China: historical reconstruction and mechanism analysis. Engineering Geology 226, 122–135.

Zhou, J., Cui, P., Yang, X., 2013. Dynamic process analysis for the initiation and movement of the Donghekou landslide-debris flow triggered by the Wenchuan earthquake. Journal of Asian Earth Sciences 76, 70–84. https://doi.org/10.1016/j.jseaes.2013.08.007